
Controller Interaction Assessment between a Full-scale Converter Wind Turbine and a MMC-HVDC Transmission System

Project Report
Elena Malz and Saioa Buruxtaga

Aalborg University
Department of Energy Technology



Department of Energy Technology
Aalborg University
<http://www.aau.dk>

AALBORG UNIVERSITY

STUDENT REPORT

Title:

Controller Interaction Assessment between a Full-scale Converter Wind Turbine and a MMC-HVDC Transmission System

Theme:

Master Thesis

Project Period:

Spring Semester 2015

Project Group:

1055/1036

Participant(s):

Elena Malz
Saioa Buruxtaga

Supervisor(s):

Massimo Bongiorno

Copies: 2

Page Numbers: 84

Date of Completion:

June 3, 2015

The content of this report is freely available, but publication (with reference) may only be pursued due to agreement with the author.

Abstract:

High voltage dc (HVDC) transmission systems are an attractive solution for connecting Offshore Wind Farms. Technology based on voltage source converters (VSCs) is the most widely accepted configuration for these applications. The introduction of the modular multi-level converter (MMC) concept adds a new level of controllability but also complexity. Recent studies have reported that a VSC could negatively interact with the system resulting in a reduced electrical damping. An input admittance matrix approach is applied to study possibility of Controller Interaction between the wind farm components. The impact of basic controller parameter design on the passivity of the subsystems is analysed. Also the net-damping criterion is applied to conclude about the total system stability.

Preface and Acknowledgements

This document is a Master Thesis in which the controller interaction between a Full-scale Converter Wind Turbine and a MMC-HVDC Transmission System is assessed. It is written by two students of the 4th semester in Wind Power Systems and High Voltage Engineering and Electrical Power Systems at the Department of Energy Technology in Aalborg University. The project was a collaboration with Chalmers University of Technology and the project was proposed by Massimo Bongiorno.

The purpose of the study is to obtain an analytical method to evaluate and conclude about the stability of an Offshore Wind Farm network (OWF) with a potential risk of controller interaction. A general case is investigated, with a 2-level voltage source converter and a Modular-Multilevel voltage source Converter (MMC) included in the OWF network.

We would like to thank our supervisor Massimo Bongiorno at Chalmers University for his guidance and great support. Also a special acknowledgement is given to his PhD students Georgios Stamatou, Selam Chernet and Ehsan Behrouzian, who helped during different steps of the project. Finally we would like to thank Florin Iov for his guidance at early stages of the thesis. Aalborg University, June

3, 2015

Elena Malz
<emalz13@student.aau.dk>

Saioa Buruxtaga-Laza
<sburuc12@student.aau.dk>

Contents

List of Figures	iii
List of Tables	viii
Nomenclature	viii
1 Introduction	1
1.1 Background	1
1.2 Problem Statement	2
1.3 Objective	3
1.4 Scope and Limitations	3
2 State of Art	5
2.1 OWF Representation for CI Assessment	5
2.2 System Modelling Approach	7
2.3 Input Admittance Matrix Concept	8
2.4 Stability Analysis Applying Frequency Domain Approach	9
2.5 Model Verification	11
2.6 Summary	12
3 System Characterisation	14
3.1 Single Line Diagram	14
3.2 Model for Stability Analysis	16
3.3 Definition of Stability in the Network	17
3.4 Summary	18
4 System Design	20
4.1 Wind Turbine - 2 Level Converter (2LC)	21
4.2 MMC - HVDC Station	29
4.3 AC System	34

4.4	Summary	36
5	System Implementation	38
5.1	Analytical Model	38
5.2	Time Domain Model	44
5.3	System Verification	45
5.4	Summary	54
6	Controller Interaction Assessment	55
6.1	Passivity Analysis of Converter Parameters	55
6.2	Stability of the Network	62
6.3	Method for System Stability Evaluation	71
6.4	Summary	73
7	Conclusion and Future Work	75
7.1	Conclusion	75
7.2	Future Work	77
	Bibliography	79
A	Appendix	83

List of Figures

2.1	Scheme of an Offshore wind farm connected to an HVDC transmission system	5
2.2	Closed-loop system formed by linear subsystems $Y(s)$ and $Z(s)$	9
3.1	Single Line Diagram of the complete OWF	15
3.2	Single line diagram of the studied system	16
3.3	Closed-loop system formed by subsystems $Y_{MMC}(s)$ and $Z_{ac-system}(s)$	17
3.4	Sign definition for the converters and the total impedance system. The current i_g is the closed-loop reference current and the P_{WT} illustrates the actual power flow.	18
4.1	Control structure of the WT-2LC including inner and outer control loops	21
4.2	AC Control Block	23
4.3	PLL control block diagram	25
4.4	Direct Voltage controller block	29
4.5	MMC model and control structure	30
4.6	Alternate Voltage Controller AVC implemented in the MMC	32
5.1	System represented by combined impedance (2LC and ac grid) and admittance (MMC)	39
5.2	Impedance of the ac-system	41
5.3	Verification of the analytical 2LC IAM means a simulation model	48
5.4	Verification of the analytical MMC IAM means a simulation model	48
5.5	Single line diagram showing the switches implemented in the time domain model	49
5.6	3-Phase Current at the IP	50
5.7	3-Phase Voltage at the IP	51

List of Figures

5.8	Reference and grid voltage v_d at IP	51
5.9	Reference and grid voltage v_q at IP	52
5.10	Reference and grid current i_d at IP	53
5.11	Reference and grid current i_q at IP	53
6.1	Poles of the the converters	56
6.2	Impact of power level on $Re[Y_{qq}]$ and $Re[Y_{dd}]$ of the 2LC. The blue dashed line demonstrates nominal values.	58
6.3	Left - Impact of current controller bandwidth on $Re[Y(s)]$ of the 2LC. Right - Impact of current controller bandwidth on $Re[Y(s)]$ of the MMC. The blue dashed line demonstrates nominal values.	59
6.4	Left - Impact of DVC bandwidth on $Re[Y_{dd}(s)]$ of the 2LC. Right - Impact of AVC bandwidth on $Re[Y(s)]$ of the MMC. The blue dashed line demonstrates nominal values.	61
6.5	Left - Impact of L on the $Re[Y(s)]$ of the 2LC. Right - Impact of C_f on the $Re[Y(s)]$ of the MMC. The blue dashed line demonstrates nominal values.	62
6.6	Closed loop representation of the evaluated system	62
6.7	Poles of $Z_{ac-sys}(s)$	63
6.8	Real parts of the studied subsystems	64
6.9	Gains of Y_{MMC} and Z_{ac-sys}	65
6.10	Left - $R_{ac-sys}(s)$; Right - $R_{MMC}(s)$	67
6.11	Net damping ($Z_{ac-sys}(s) + Z_{MMC}(s)$)	68
6.12	Impact of parameter variation over the stability of the system according to net-damping criterion	69
6.13	Simulation results when inserting a reference voltage step on the MMC side	70
6.14	Flow chart of analytical method for evaluation of origin of instabilities	72
A.1	Phasors $\alpha\beta$ to dq transformation	83

List of Tables

4.1	Summary of the design parameters of both converters	33
4.2	Cable data for each array branch and the aggregated total impedance of all 6 arrays [1].	35
4.3	Left - Parameter of one single transformer. Right - Resulting para- meter for parallel connection	36

Nomenclature

Acronym	Description
ACC	Alternate Current Controller
AVC	Alternate Voltage Controller
CI	Controller Interaction
DVC	Direct Voltage Controller
HVAC	High Voltage Alternate Current
HVDC	High Voltage Direct Current
IP	Interface Point
ML	Multilevel
MMC	Modular Multilevel Converter
OWF	Offshore wind farm
PI	Proportional Integral
PLL	Phase Locked Loop
PMSG	Permanent magnet synchronous generator
SISO	Single Input Single Output
SPWM	Sinusoidal Pulse Width Modulation
SM	Sub Modules
WT	Wind Turbine
XLPE	Cross-linked polyethylene

List of symbols

Overall system

Symbol	Description
$Y_{MMC}(s)$	Transfer function of MMC
$Y_{MMC}^m(s)$	IAM of MMC
$Y_{2LC}(s)$	Transfer function of the WT-2LC
$Y_{2LC}^m(s)$	IAM of the WT-2LC
$Z_{ac-system}(s)$	Transfer function of aggregated ac-system
S	Apparent Power
P	Active Power
Q	Reactive Power
Δ	Small signal value

WT-2LC symbols

Symbol	Description
P_{vsc}	Active power flowing into the 2LC
P_{WT}	Active power flowing generated by WT
P_{cap}	Power absorbed by dc-link capacitor
Q_0	Reactive power controlled
i_q^*	q -channel reference current
i_d^*	d -channel reference current
v_{dc}	dc-link voltage in the
v_c	Voltage at terminals
$v_{c,dq}^*$	Reference voltage at terminals in dq -frame
$v_{g,dq}$	Measured grid voltage after filter L_f in dq -frame
v_{abc}^*	Reference voltage input for SPWM abc -frame
L_f	Line filter
C_{dc}	Capacitor in dc-link
ω_g	Network frequency low-voltage side
θ_g	Grid voltage phase angle
α_f	Low pass filter of the ACC bandwidth
α_c	ACC bandwidth
α_{PLL}	PLL bandwidth
α_d	DVC bandwidth
$H(s)$	ACC Low pass filter transfer function
$F_{PI}(s)$	ACC PI controller transfer function
$G_c(s)$	Closed-loop transfer function of the ACC
$Y_i(s)$	IAM of the ACC
$G_{PLL}(s)$	PLL transfer function
$H_{dc}(s)$	DVC Low pass filter transfer function
$G_{dc}(s)$	Transfer function i_d^* to measured $v_{g,dq}$

MMC symbols

Symbol	Description
i_t	Current at the terminals
i_g	Current flowing to the OWF network
i_{Cf}	Current flowing into the IP capacitor
v_t	Measured voltage at the terminals
$v_{t,dq}^*$	Reference voltage at the terminals in dq -frame
$v_{IP,dq}$	Measured grid voltage after at IP in dq -frame
L_{fm}	Filter total inductance
R_{fm}	Filter total resistance
C_f	IP capacitor
L_{arm}	Arm inductance
R_{arm}	Arm resistance
α_{cm}	ACC bandwidth
α_{vm}	ACV bandwidth
α_{fm}	Low pass filter of the ACC bandwidth
α_{fv}	Low pass filter of the ACV bandwidth
$H_{ac}(s)$	ACC Low pass filter transfer function
$G_{ac}(s)$	ACC PI controller transfer function
$G_{cm}(s)$	Closed-loop transfer function of the ACC
R_{gc}	ACC virtual damping term
$G_{vc}(s)$	AVC PI controller transfer function
$H_{vc}(s)$	AVC Low pass filter transfer function
R_{gc}	AVC virtual damping term

1 Introduction

1.1 Background

Wind power penetration into current power systems is rapidly increasing [2]. A recent trend is to install big offshore wind farms (OWF) since their energy generation is higher as compared to onshore installations.

Due to the limitations of power transmission using high voltage ac (HVAC) cables, OWFs have been usually installed close to shore [2, 3]. It is expected that in the next years wind industry will install OWFs further from the shore aiming for higher energy yields [4].

High voltage dc (HVDC) transmission systems are an attractive solution for these cases, since they not only eliminate issues related with long ac transport cables but also enable an asynchronous operation of the offshore grid [3]. HVDC technology based on voltage source converters (VSCs) is the most widely accepted configuration for offshore applications [2, 5]. While there are three main topologies for VSC-HVDC systems commercially available, i.e. two-levels (2LC), three-levels (3LC) and multi-level (MLC) converters, nowadays only the latter is considered for OWF dc connection to the main grid [4]. The recent deployment of ML-VSC for HVDC transmission is linked to the introduction of the modular multi-level converter (MMC) concept in [6], which offers scalability of voltage ratings with low switching losses. Thus, with this topology it is easier to construct VSCs with very high power and voltage ratings. However, the experience with the operation of MMC in HVDC systems is limited and its dynamic interaction with the power system has not yet been fully modelled [7].

The interaction between a VSC and power system is given by the control strategy of the VSC and its parameters. Pure electrical interactions between the VSC controllers and the network are known as control interaction (CI) [8]. Recent studies have reported that a VSC could negatively interact with the system resulting in a reduced electrical damping [5, 9, 10]. Therefore, the integration of these elements

into electric networks increases the risk for local instabilities starting from poorly damped oscillations [11].

Moreover, at the same time that MMC-HVDC transmission systems are being introduced in OWF projects, the full-scale VSC wind turbine (WT) , i.e. type-4, is gaining general acceptance for offshore installations. Hence, it can be expected that future OWF will be comprised by a large number of VSCs which will interact with the network nearby and could potentially lead to instabilities in the system. A number of publications focus on the analysis of the interaction between a VSC and the grid on the controller level [5, 12, 9, 10]. However, CI between the VSCs incorporated in a certain system is a recent topic of research. CI between the VSCs of doubly fed induction generator (DFIG) WTs and the MMC of an HVDC-based transport system has been studied under electromagnetic transients (EMT) conditions in [13]. In [5] the authors present a study of stability and resonance problems in OWF comprised by type-4 WTs and connected to the main grid through a 2LC-based HVDC system. However, in the public domain, there is not yet a study that evaluates the possibility of CI between an MMC-based HVDC system and the rest of a wind farm where type-4 WTs are connected.

1.2 Problem Statement

The short operational experience with MMC-HVDC systems for offshore applications has not publicly revealed yet serious instability problems on the controller level. However, according to [7, 13] and to the theory behind VSC-grid interaction stability [10], the MMC-VSC technology applied in HVDC systems can potentially lead to CI issues with other elements in the system, as other VSCs or transmission systems.

Therefore, this thesis aims to asses the possibility of CI within an OWF network with type-4 WTs and a MMC-HVDC transmission system. An appropriate and accurate model of both converters technologies is required to study these interactions in the network. The use of small-signal models provides a deeper insight into the dynamics of the converters and the network itself [5, 4]. The stability of the system will be assessed by using appropriate tools that allow identifying the origin of possible instabilities.

1.3 Objective

The major goal is the development of a methodology that can offer a systematic approach for the investigation of possible instabilities in an OWF network with different VSCs technologies. Further objectives are given as:

1. Derive the control structures of the MMC and 2LC.
2. Derive the input admittance matrix (IAM) of the 2LC and the MMC.
3. Evaluate analytically the influence of the controllers parameters in the MMC IAM and 2LC IAM .
4. Assess the possibility of CI between the converters and the ac network applying proper analysis tools.

1.4 Scope and Limitations

The studies presented in this report are formulated for steady state conditions. Therefore, several assumptions and simplifications are taken in the modelling of the individual elements in the OWF, allowing an easier but proper analysis of the possibility of interactions in the network.

The studied OWF is not based on any particular existent wind farm project. The OWF network layout and the design of its components is based on general engineering rules and information available in the public domain. Moreover, no in force regulation has been found for power quality requirements within the OWF and up to the offshore connection point of it with the HVDC station.

An important assumption that allows a simplified model of the OWF network, is that the dc links in both ac-to-ac converters totally decouple the dynamics between the wind farm transmission system and the elements after the dc connection. That is:

- For the WT full-scale back-to back-converter, only the interactions between grid side 2LC and the OWF network are considered.
- For the HVDC transmission system, only the interactions between the offshore station and the OWF network are considered.

Another assumption with great impact in the study of interactions in such network, is the role that each of the converters have in the operation of the system in steady state conditions. According to their function, the controllers implemented in each of the converter are defined. In this project the following is assumed:

- The 2LC must control the dc link voltage and inject the power generated by the WT into the transmission system. It is supposed that the WT generator-side converter controls the power injected in the dc link. This side of the back-to-back converter is then modelled as a constant current source.
- The offshore HVDC station -with MMC technology- must give the reference frequency and magnitude voltage for the whole OWF. Hence, it should keep a stiff voltage at the connection point with the OWF network.

2 State of Art

The focus of this Chapter is laid on the review of the theory, methods and assumptions that will allow the investigation of possible CI between type-4 WT 2LC and the MMC-based HVDC transmission system of an OWF operating in steady state conditions.

2.1 OWF Representation for CI Assessment

As mentioned before, it is expected that new OWF will be located far from shore and hence, that the transmission of the generated power to the main grid will be done through an HVDC system. At the same time, type-4 WTs are gaining widespread acceptance in high-power applications as the ones projected for OWFs. Fig. 2.1 shows an schematic representation of an OWF network with these characteristics.

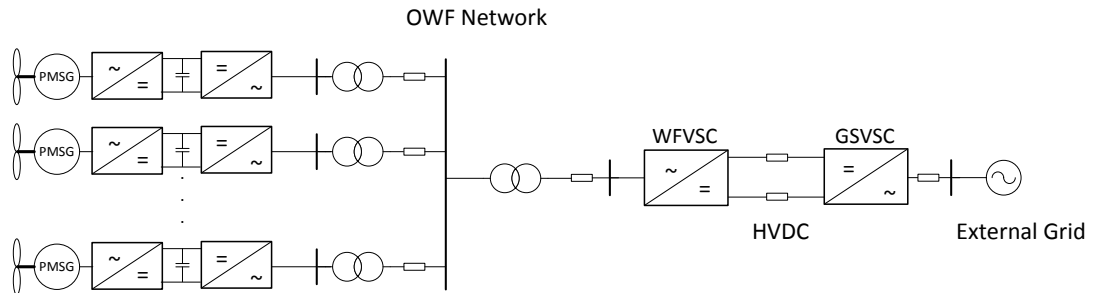


Figure 2.1: Scheme of an Offshore wind farm connected to an HVDC transmission system

The following describes a possible operation of such network in steady state condition.

The onshore VSC (GSVSC) of the HVDC system is controlled to keep the dc voltage constant whereas the wind farm side VSC (WVSC) is responsible of collecting the energy produced in the OWF and send it to the main grid through the dc link. The WVSC operates as a voltage source with constant frequency, voltage magnitude and phase angle [3, 14], setting the frequency and voltage at the ac collection bus.

Looking at the WT, the generated power is fully controlled by the back-to-back power converter that decouples the generator from the OWF grid [15]. Due to the decoupling, in steady-state conditions the generator terminal voltage and frequency do not affect the collection grid [16] and the active power generated by the PMSG flows through the inverter to the ac grid. In this way, the generator-side converter controls the power produced by the PMSG, whereas the grid-side inverter controls the dc link voltage.

In this way, ac dynamic interactions will only exist between the WVSC, the ac grid and the inverter of the full-scale converter in the WT. Moreover, these interactions between the VSCs and the network are determined by the VSCs control strategies and parameters [12].

Original controls of power converters are considered highly confidential for all manufacturers and thus the controls are not necessarily available to all parties involved in the wind farm project [13]. This sets a risk for interactions on the controller level between the elements in the network.

In [5], it is proven that CI both, below and above the fundamental frequency, may occur in 2LC based HVDC systems. However, as previously mentioned, the possibility of CI with MMC-HVDC is still an open question. To investigate CI, the elements in the network under consideration must be adequately modelled to capture the electric dynamics that can influence the stability of such a system in the interested frequency range.

In [17, 18] the WTs of the OWF are aggregated into a single unit where the lumped WT is rated at the OWF power and is modelled as a current source, that emulates the generator and the turbine side converter, and a two-level converter connected to the ac collection grid. The dynamic interaction between the OWF network and the HVDC system, are studied in [17] by modelling the WVSC with its correspondent controllers but neglecting the dc link and GSVSC dynamics and therefore connecting the WVSC to a big capacitance providing a stiff dc voltage.

2.2 System Modelling Approach

Interactions between VSCs and power networks can be analysed by applying a state-space approach or an impedance-based approach.

In the state-space approach, the individual modes of the elements in the network are combined to an overall system model expressed in matrix form. Based on this model the stability and the dynamics of the systems can be evaluated through the eigenvalues of their matrices, which give information about the oscillatory properties of the system at a certain state [19, 20, 21].

On the other hand, with the impedance-based method the model of the power system under study is constructed based on the impedance matrices of the different elements in the system. Accordingly, the impedance matrices of each element represent submodels of the main system. By using this method, the stability of the system can be investigated through the analysis of the passivity properties of each of these individual submodels [20, 22]. Furthermore, Nyquist criterion can be applied to the system model to determine the overall stability in those cases where the submodels turn to be non-passive. In this way, this analytical method facilitates the characterization of the influence of different circuit and control parameters on the overall system stability [17]. Therefore, when modelling VSCs with this approach adaptive design methods can be easily applied in the individual subsystems to guarantee stability in the system [17, 22].

In [20], the dc network dynamics of VSC-HVDC system is assessed through both, eigenvalues in the state-space model and frequency-domain approach based on the impedance. According to the author, the eigenvalues analysis is helpful to assess the influence of different parameters on the dynamic performance of the system, but no clear information about the origin of instabilities can be obtained. Only by evaluating the system through a frequency-domain analysis, the author finds the exact factors that turn the system unstable. *Harnefors et. al* in [10, 22], and *Liu et.al* in [5], also apply this frequency domain approach to investigate the nature of instabilities in power systems with connected VSCs.

2.3 Input Admittance Matrix Concept

With the impedance-based approach an electric power system can be modelled through the impedance matrices of the components in the network. A transformation of the system in the dq -synchronous frame, limits the system to two channels d and q [23]. After linearisation, the electrical system response to small disturbances can be described in terms of its differential input admittance matrix $Y(s)$ as

$$\Delta i = Y(s) \cdot \Delta v \quad (2.1)$$

where Δv and Δi are small voltage and current perturbations around the singular point. Henceforth $Y(s)$ will be simply referred as IAM.

The opposite case in which Δi is the input and Δv the output, the system can be analysed with the help of an impedance matrix ($\Delta v = Z(s) \cdot \Delta i$).

In [5, 10, 22] the impedance or admittance characteristics of a VSC is given by the implemented controllers and its parameters. Since the control is carried out in the dq -frame, the general form for an IAM is defined in the converter synchronous frame as

$$Y(s) = \begin{bmatrix} Y_{dd}(s) & Y_{dq}(s) \\ Y_{qd}(s) & Y_{qq}(s) \end{bmatrix} \quad (2.2)$$

The inverse of this matrix results in the OIM and can be described as

$$Z(s) = Y^{-1}(s) = \begin{bmatrix} Z_{dd}(s) & Z_{dq}(s) \\ Z_{qd}(s) & Z_{qq}(s) \end{bmatrix} \quad (2.3)$$

In studies such as [20] the converter in itself is assumed as ideal and lossless, so the IAM is based solely on the transfer function of the controllers and the output filter. Depending on the frequency range in which the interactions are studied, different controller types have to be taken into account or can be neglected.

If simplifying the system and considering only the current controller, the transfer matrix of a VSC is symmetric as seen in [22]. However, transfer matrices become

dq non-symmetric if the outer control loops are included [23].

The IAM of a typical 2L-VSC has been calculated in several publications for different implemented controllers for the investigation of stability issues [9, 17, 10, 5, 20]. On the other hand, the IAM of an MMC is not yet available in the public domain.

2.4 Stability Analysis Applying Frequency Domain Approach

If a system can be modelled by a closed-loop SISO system, as the system in Fig. 2.2, its stability can be assessed by studying the frequency response of the subsystems $Z(s)$ and $Y(s)$ [11]. Two frequency domain tools can be considered for this analysis: the passivity approach and the net-damping criterion.

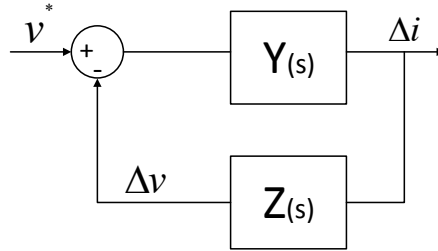


Figure 2.2: Closed-loop system formed by linear subsystems $Y(s)$ and $Z(s)$

2.4.1 Passivity of closed-loop transfer function

The stability of a SISO feedback system can be analysed through the frequency response of the individual linear systems $Z(s)$ and $Y(s)$. Taking $Z(s)$ as an example, this subsystem can be defined as *passive* if and only if,

1. $Z(s)$ is stable
2. $Re [Z(j\omega)] \geq 0$ for every $\omega \geq 0$

Moreover, $Z(s)$ is said to be *dissipative* if $Re [Z(j\omega)] > 0$ for every $\omega \geq 0$.

Extending the approach to the evaluation of the total system, the passivity of a closed-loop systems can be assessed in a similar way. The closed-loop transfer function of the system in Fig.2.2 is given by Eq. 2.4

$$G(s)_{cl} = \frac{Y(s)}{1 + Y(s) \cdot Z(s)} \quad (2.4)$$

If both subsystems $Y(s)$ and $Z(s)$ are stable and passive then $G(s)_{cl}$ is also stable and passive. However, the opposite is not true. If one of the subsystems is non-passive, or even if both of them are non-passive, then $G(s)_{cl}$ is not necessarily unstable, or non-passive [11]. For this cases where a clear conclusion about the stability can not be drawn, the Nyquist criterion can be applied to provide a final conclusion about the closed-loop system stability.

2.4.2 Net-damping-stability criterion

According to [24], this criterion is valid for analysing the stability of systems as the one shown in Fig. 2.2. By applying the Nyquist criterion to the open-loop transfer function of the controlled process, the net-damping-criterion can be derived as following. Eq. 2.5 is the open-loop function of the system in Fig. 2.2

$$G(j\omega)_{ol} = Z(j\omega) \cdot Y(j\omega) \quad (2.5)$$

where the individual subsystems are defined as

$$Z(j\omega) = R_z(\omega) + jX_z(\omega), \quad \frac{1}{Y(\omega)} = R_y(\omega) + jX_y(\omega) \quad (2.6)$$

Then, Eq. 2.5 can be rewritten in

$$\begin{aligned} G(j\omega)_{ol} &= \frac{R_z(\omega) + jX_z(\omega)}{R_y(\omega) + jX_y(\omega)} \\ &= \frac{R_z(\omega)R_y(\omega) + X_z(\omega)X_y(\omega)}{R_y^2(\omega) + X_y^2(\omega)} + j \frac{R_y(\omega)X_z(\omega) - R_z(\omega)X_y(\omega)}{R_y^2(\omega) + X_y^2(\omega)} \end{aligned} \quad (2.7)$$

According to Nyquist criterion $G(j\omega)_{ol}$ is stable if the curve if $Z(j\omega) \cdot Y(j\omega)$ does not encircle the $-1 + j0$. To determine whether the Nyquist plot of $G(j\omega)_{ol}$ encircles this point, its imaginary part is set to zero $Im [Z(j\omega) \cdot Y(j\omega)] = 0$. The

frequencies at the points when the imaginary part becomes zero, are the resonance frequencies and are from now on expressed as ω_{res} . From Eq.2.7 it is seen that $R_y(\omega_{res})X_z(\omega_{res}) - R_z(\omega_{res})X_y(\omega_{res}) = 0$ and, in turn

$$\frac{R_z(\omega_{res})}{R_y(\omega_{res})} = \frac{X_z(\omega_{res})}{X_y(\omega_{res})} \quad (2.8)$$

Inserting the expressions Eq. 2.8 in 2.7 yields to 2.9, which gives the possible intersections of the Nyquist curve with the real axis.

$$Z(j\omega_{res}) \cdot Y(j\omega_{res}) = \frac{R_z(\omega_{res})}{R_y(\omega_{res})} \quad (2.9)$$

In this way, if $Z(j\omega_{res}) \cdot Y(j\omega_{res}) > -1$ then $R_z(\omega_{res}) + R_y(\omega_{res}) > 0$, guaranteeing that the Nyquist plot does not encircle $-1 + j0$. However, Eq. 2.9 accounts only when $R_y(\omega_{res}) > 0$. This stability criterion is known as *positive-net-damping*. On the contrary, if $R_y(\omega_{res}) < 0$, the *negative-net-damping* stability criterion applies, which is given by

$$\frac{R_z(\omega_{res})}{R_y(\omega_{res})} < -1 \longrightarrow R_z(\omega_{res}) < -R_y(\omega_{res})$$

$$R_z(\omega_{res}) + R_y(\omega_{res}) < 0 \quad (2.10)$$

Compared to the passivity analysis initially described, a great advantage of the net-damping-criterion is that there is no need for each of the subsystems $Y(s)$ and $Z(s)$ to be passive or even stable by itself in order to provide a definite answer about the stability of the closed-loop system [11].

2.5 Model Verification

Two verifications are needed to confirm the effectiveness of the approach in the assessment of CI between VSCs in a network: impedance-based models verification and analytical stability results verification.

The analytical results of the frequency-domain stability analyses can be validated by time-domain simulations. As deduced from [5, 17, 20, 10], depending on the focus of the study there exist different approaches for evaluating the results in time-domain .

In [10, 22] the converter-grid interaction analysis is carried out based on the IAM of the VSC and the impedance matrix of the grid. To this aim, the authors evaluate the impact of different controller parameters over the impedance characteristic of the VSC. Hereby, the dissipative properties of this submodel can be assess. Time-domain simulations verify the impact of the parameters over the stability of the system, proving that oscillations are built according to what is predicted through the analytical equations.

In [5, 17], the stability of an OWF network with type-4 WT and 2L-VSC based HDVC system is assessed by applying Nyquist for different power inputs/outputs of the VSCs. It is found that under certain power transfer levels the stability of the system could not be ensured. The existing instability at the specified power level is verified by means of time domain simulations by moving the system from a stable power transfer condition to the one found to turn the system unstable. In the time domain simulation the instability is shown as an oscillation undamped by the controllers of the VSCs in the network.

In [20] the author applies frequency domain approach to analyse the passivity properties of a VSC-HVDC system and its dc grid subsystem. To this aim, the impedance characteristics of both subsystems under different conditions of power transfer, dc cable length, and ac grid stiffness are compared and the situations possibly leading to system instabilities are identified. Time domain simulations reproduce this instability conditions and evaluates the system response with different control strategies of the VSC-HVDC system.

2.6 Summary

This Chapter gives an overview of methods applied in the stability assessment of power systems with connected VSCs. The frequency-domain approach based on impedance models is considered to be the best modelling tool for the assessment of CI proposed in this thesis. The OWF network can be modelled through the equivalent impedance or admittance matrices of the individual subsystems, i.e.

aggregated WT-2LCs, ac network and the rectifier module of the MMC-based HVDC system.

It is highlighted that, whereas several publications have derived an IAM of a 2L-VSC, an IAM of a MMC is not yet documented. The IAM of the converters is shaped by the implemented controllers. Depending on the frequency range of interest for the analysis different controller types must be taken into account. In this project the investigated frequency is limited by the lowest controller bandwidth in the system and certain number of harmonic within which the resonance frequency of the OWF transmission network can be found. In this case the study frequency range is chosen to capture the lowest controller bandwidths (PLL) up to possible cable resonance frequencies.

In this study the passivity evaluation and the net-damping criterion are the tools applied in the analysis of the stability of the system. Furthermore, it is indicated that verification of the analytical models is needed in order to determine the effectiveness of the model to assess CIs.

3 System Characterisation

This Chapter is dedicated to the description of the system evaluated in this project, highlighting the main assumptions and simplifications made. To have a clear image of the studied system a single line diagram is presented including all implemented and modelled components. Further on it is described how the SISO representation of this OWF is obtained. This divides the total system into two subsystems, which can be evaluated either individually or as open and closed loop. order to study a closed loop and allow studies on stability and possible interactions. In order to clarify the definition of stability in this thesis another section is added explaining the prerequisites as sign conventions for studying the system in a closed loop.

3.1 Single Line Diagram

This section is dedicated to the description system and should clarify the simplifications which have been made to analyse interactions in the network. A figure of the entire OWF is shown in Fig. 3.1, where the dashed line represents the limits of this studies. The shaded part, showing the HVDC line and the onshore transformer are not taken into consideration in this thesis.

For the studies here presented, a benchmark OWF is designed taking into account general engineering rules for OWF design. Without loss of generality, the OWF network presents a simple layout enough to carry out the stability investigation in this project. Moreover, no power quality regulations applicable *within* the OWF have been found. It is of the authors understanding that the European Network of Transmission System Operators for electricity (ENTSOe) is currently preparing a draft for network codes regarding to HVDC connected WF. However these codes are still under review and hence, not yet followed [25] [26].

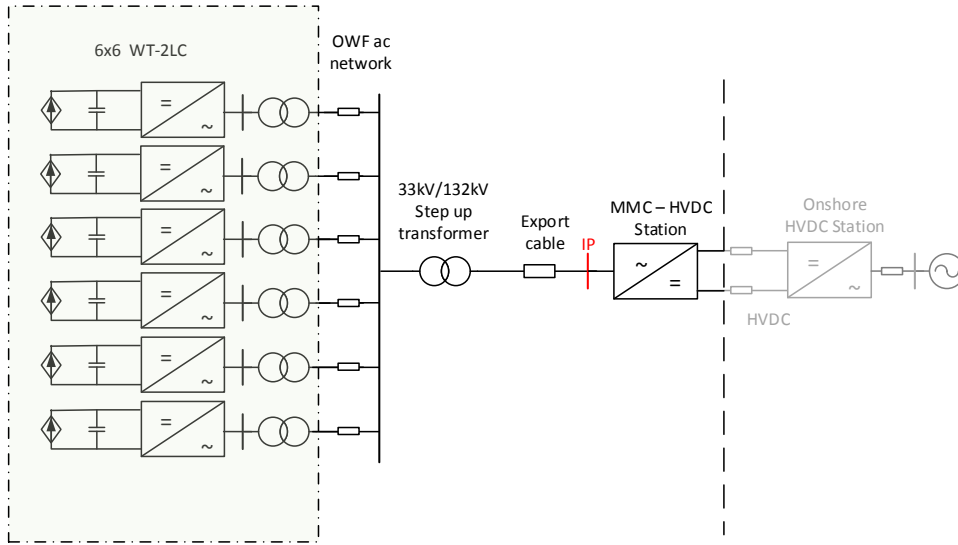


Figure 3.1: Single Line Diagram of the complete OWF

It is assumed that the OWF is comprised by 36 variable speed WTs with full-scale power conversion and a rated power of 5 MW which are radially connected to a 33 kV busbar. A current source represents the generator and the turbine side converter of each WTG. The network layout is shown in Fig. 3.1. By applying the modelling approach reviewed in section 2.2, the 36 WTs are lumped into a single generation unit with 180 MW rated power. For simplification, the transformer of the WT is neglected and hence it is assumed that the the generated power is directly injected in the 33 kV network.

The OWF ac network is aggregated into a single π -model according to the standards given in [27] for the collector and feeder levels. The equivalent feeder is connected to the offshore substation that boosts the voltage level to 132 kV. Following the recommendations in [28], for reliability reasons it is proposed that in the offshore substation two transformers operate in parallel to ensure power transmission from OWF to the main grid in case of outages. Fig. 3.1 shows a single transformer which represents the parallel connected units. According to [29] for submarine cables above 30 km reactive power compensation is necessary. The reactive current which would be needed from the HVDC system would fully load the cable leaving no room for active power transmission. This parameter is variable and can be changed in the model. Also this cable is represented as a π -model in this study case. Finally, the HVDC offshore station is based on MMC operates as a voltage source with constant frequency and voltage magnitude, setting this values at the

interface point (IP), where the export cable connects the OWF with the HVDC station. Assuming total decoupling from the dc transmission system, the onshore HVDC station and the dc link are represented as a constant voltage source.

The simplified model of the studied OWF is shown in Fig. 3.2. The lumped WT generation unit is identified as WT-2LC and the line reactance is simply the output filter of the converter. The export cable and OWF ac network are already represented by the equivalent π -model.

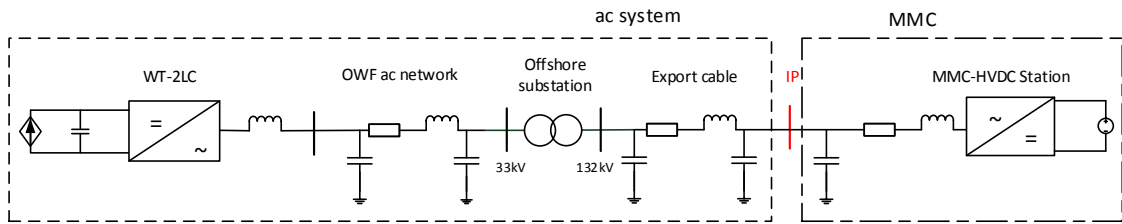


Figure 3.2: Single line diagram of the studied system

In this project possible interactions between the two systems are enclosed by the dashed boxes in Fig. 3.2. Further explanation about this defined subsystems can be found in the next section.

3.2 Model for Stability Analysis

One of the aims of this report is to develop a methodology which can describe and predict the possible occurrence of instabilities in the OWF network. According to the theory given in the state of art (2.4), the stability of the closed-loop system of the studied network can be assessed through the frequency response of the transfer functions of the subsystems. To this aim, a SISO representation of the previous described OWF model is derived and shown in Fig. 3.3 has to be derived. The Figure shows the closed-loop system evaluated in this project where $Y_{MMC}(s)$ represents the transfer function of the MMC-HVDC station, and $Z_{ac-system}(s)$ the aggregated impedance of the WT-2LC including the ac-system up to the IP. The exact elements which are included in the subsystems have been displayed in the previous section in Fig. 3.2.

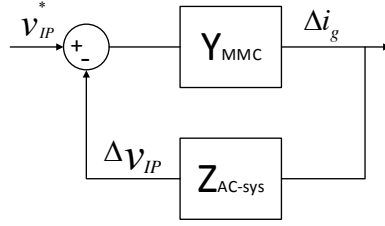


Figure 3.3: Closed-loop system formed by subsystems $Y_{MMC}(s)$ and $Z_{ac-system}(s)$

The MMC transfer function $Y_{MMC}(s)$ and the 2LC transfer function, $Y_{2LC}(s)$ - included in the aggregated $Z_{ac-sys}(s)$ - as well as their matrices $Y_{MMC}^m(s)$ and $Y_{2LC}^m(s)$ can be derived from the small signal representation of the controller dynamics. The superscript m is added, when referring to the matrices representation. In this way, $Y_{MMC}(s)$ and $Y_{MMC}^m(s)$ represent the same system and consequently the same stability properties. The big advantage of having both expressions of the same system are the various possibilities of analyses dependent on the field of interest. The stability-criterion can be applied to a single transfer function $Y_{MMC}(s)$, but in case of instability an analysis of the IAM $Y_{MMC}^m(s)$, facilitates the detection and understanding of its origin. Logically, the same applies for $Y_{2LC}(s)$ and $Y_{2LC}^m(s)$.

3.3 Definition of Stability in the Network

Having the closed-loop system in Fig. 3.3, the $Y_{MMC}(s)$ is derived by assuming that current i_g flows out of the converter, and consequently the $Z_{ac-system}(s)$ is derived by assuming that i_g flows into the subsystem. Looking closer into the operation of the network, as described in section 3.1, it can be noticed that the current flow of i_g will naturally be opposite to what is defined for the closed-loop system in Fig. 3.3, since the power generated by the WT will flow through the ac-system into the HVDC system.

These different flows definitions should not confuse the reader in the different stages of design, implementation and analysis of the network. Independently from the actual power flow direction and the IAM design, the network stability assessment should be consistent with the closed-loop definition in Fig. 3.3. Figure 3.4 is added to state the different sign conventions and provide a better understanding about this issue. The three blocks represent the subsystems that conform the power

network and the sign convention under which they are derived. The current i_g represents the closed-loop flow definition and P_{WT} and i_{WT} the OWF network natural flow.

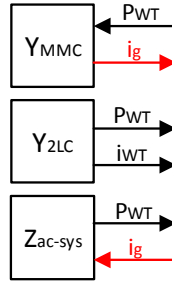


Figure 3.4: Sign definition for the converters and the total impedance system. The current i_g is the closed-loop reference current and the P_{WT} illustrates the actual power flow.

The positive or negative impedance appearance of a component or subsystem is strongly related with the defined sign convention. This may limit the application of the passivity approach for determining the stability of the network since, according to the definitions in 2.4.1, the close-loop system in Fig. 3.3 can only be passive if both subsystems $Y_{MMC}(s)$ and $Z_{ac-system}(s)$ are passive, i.e. stable and with a positive real part for $\omega \geq 0$.

For these cases where the passivity approach is not applicable, a different criterion should be followed to draw conclusions about the stability of the studied network. As described earlier, with the net-damping-criterion the stability of the closed-loop system can be determined even if both subsystems $Y_{MMC}(s)$ and $Z_{ac-system}(s)$ are non-passive or even unstable. In [11] it is argued that in a controlled process both subsystems can be individually unstable, but that by closing the loop through the negative feedback the system can get stabilised.

3.4 Summary

This chapter presents the studied system with the help of a single line diagram. The characteristics of the individual parts are described to give a clearer understanding of the study case. Also a introduction of later stability studies is given by presenting the method of transferring the single line diagram into a SISO closed loop system.

In order to not confuse the reader with current flow conventions or other definitions it is stated how initial definitions can influence later conclusions in terms of system stability.

4 System Design

The controller design is a crucial part of the general system layout, since instability can often find its origins in wrongly designed controllers.

The evaluated system is divided into 3 subsystems, the WT-2LC, the ac grid system and the MMC.

Based on the assumption that converters are often designed by different manufacturers and combined on-site, the parameters of the controllers of the 2LC and the MMC are chosen independently. Therefore, in the selection of the parameters of the 2LC it is assumed that no information is given about the the MMC control, and vice versa.

It can be noticed through reading that controllers implemented in the 2LC are explained really detailed, whereas the controller structure of the MMC is held rather shortly. The reason for this is the similar design approach for the MMC current controller. Additionally, the alternating voltage controller of the MMC is based on a related mathematical procedure and has therefore not to be described such detailed.

It is worth mentioning that the selection of controller parameters is based on the referred publications.

Three phase power systems are defined by time-varying voltages and currents, what restrains a direct application of the conventional small-signal linearisation methods. To overcome this problem, a steady state system can be modelled in a rotating dq -reference frame where sinusoidal variables at the fundamental frequency become dc quantities and the system can be linearised at an operation point to develop a small-signal linear model [30]. A more detailed explanation to the $dq0$ transformation can be found in the Appendix A1.

In [20, 22] small-signal modelling in a rotating dq -reference frame is proven to be

a suitable approach. It successfully captures the system dynamics under small disturbances of a balanced network with connected VSCs by applying impedance and state-space models.

4.1 Wind Turbine - 2 Level Converter (2LC)

In type-4 WTs the back-to-back converter decouples the turbine rotor from the grid what allows a rotor speed independent of the grid frequency ω_g ($2 \cdot \pi \cdot 50Hz$). It is assumed that the power flow is always downstream, from the power generation to the grid. Consequently, the generator side works as a rectifier, while the grid side converter can be seen as an inverter. In the most WT back-to-back converter solutions, 2LC are implemented due to the robust performance and relatively simple control structure [31]. The rectifier is responsible for the active power control, regulating the power extracted from the wind turbine rotor. In this study the rectifier is represented simply as a current source, assuming constant power input and a decoupled system [18].

In Fig. 4.1 the control blocks of the total inverter control are shown.

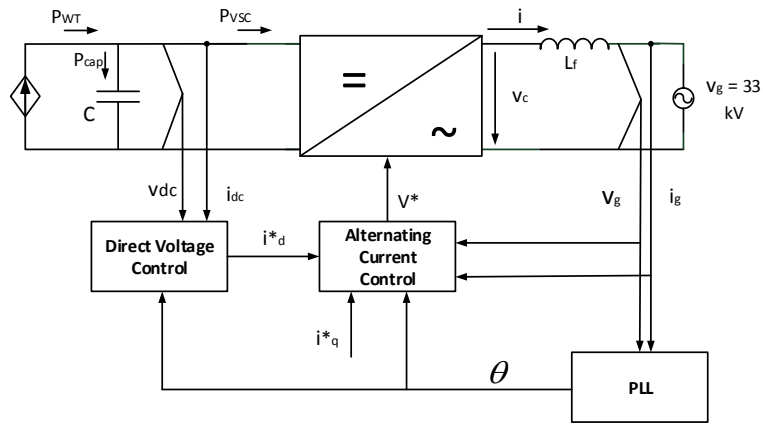


Figure 4.1: Control structure of the WT-2LC including inner and outer control loops

The control structure can be divided into an inner and an outer loop. The inner loop is the alternating current control (ACC) loop, which creates the reference voltage V^* for the sinusoidal pulse width modulation (SPWM) applied to the converter. Outer loops include the PLL and the direct voltage control (DVC). The reference current i_q^* is taken as a constant and the reference current in the d -entry i_d^* is given by the DVC.

The active power P_{WT} generated by the WTs, flows in the converter (P_{vsc}) and partly into the DC link for balancing purposes. In case of a dc-voltage v_{dc} unequal to the set voltage, the power P_{cap} is absorbed by the capacitor. On the ac side, downstream of the converter, for simplification reasons a pure line reactance L_f is considered for filtering high frequency harmonics.

As it was explained previously, the converter is representing a lumped converter for the whole OWF. Hence, the voltage at the converter terminals is already 33 kV , the operating voltage of the collection grid. Outer loops are at least 10 times slower than the current control loop since their output is the reference value for the ACC [32, 22]. For simplicity, the converter in itself is assumed as lossless and without any computation or switching delays [22].

4.1.1 Alternate Current Control (ACC)

The ac side voltage equation can be set up as

$$v_c = v_g + j\omega L_f + L_f \frac{di}{dt} \quad (4.1)$$

what can be derived from Fig. 4.1

To control the voltage v_c at the terminals of the converter the ac controller can be defined as

$$v_{c,dq}^* = \left(k_p + \frac{k_i}{s}\right)(i_{dq}^* - i_{dq}) \pm \omega L_f i_{qd} + \frac{\alpha_f}{s + \alpha_f} v_{g,dq} \quad (4.2)$$

A control block of Eq. 4.2 is shown in Fig. 4.2. Input values for the ACC are the measured grid quantities $i_{g,abc}$ and $v_{g,dq}$ as well as the reference currents i_{dq}^* given by the outer control loops. The measured grid current i_g is transformed to the converter dq -reference frame and compared with the reference current i_{dq}^* . This error is the input of the PI controller, which design is explained later on. In Eq. 4.2 cross coupling between the dq currents can be noticed, what is also shown in the control block diagram in Fig. 4.2. For a better controller operation, grid voltage $v_{g,dq}$ is fed forward, but due to possible grid disturbances a low pass filter with the bandwidth of α_f is added [22]. The output v_{abc}^* is the reference for the SPWM of the switching operation.

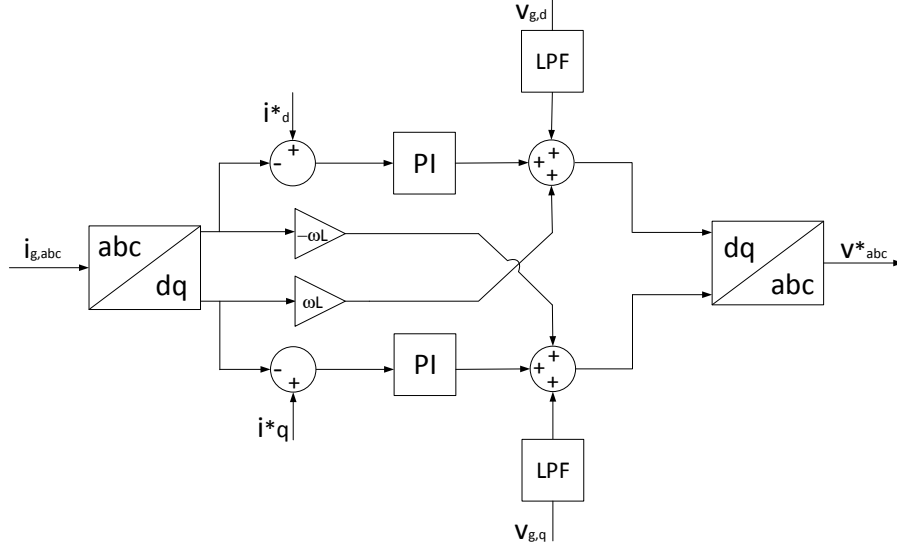


Figure 4.2: AC Control Block

The reference current i_q^* is controlled to zero under the assumption that no reactive power compensation is required by the WT generation unit on the OWF network [25] [26]. The reference current i_d^* is generated by the DVC later explained in subsection 4.1.3.

The current control loop is assumed much faster than the outer loops and reacts instantly to a set voltage reference. In this way, if the delay time T_d due to computation and switching is neglected, it can be assumed that

$$v_c = e^{-sT_d} \cdot v^* = v^*. \quad (4.3)$$

Thus the the two equations 4.1 and 4.2 can be connected as

$$v_c = v^* = F_{PI}(s)(i^* - i) + j\omega_g L_f \cdot i + H(s) \cdot v_g \quad (4.4)$$

where $H(s) = \frac{\alpha_f}{s + \alpha_f}$ represents the low pass filter and $F_{PI}(s) = k_p + \frac{k_i}{s}$ the PI controller.

The equation 4.4 can be transformed to the dq -reference frame and rearranged to

$$i_{dq} = G_c(s)i_{dq}^* + Y_i(s)v_{g,dq} \quad (4.5)$$

where $G_c(s)$ and $Y_i(s)$ are the closed-loop transfer functions and the current controller input admittance respectively [22]:

$$G_c(s) = \frac{k_p s + k_i}{L_f s^2 + k_p s + k_i}, \quad Y_i(s) = -\frac{s^2}{(L_f s^2 + k_p s + k_i)(s + \alpha_f)} \quad (4.6)$$

Based on [33] the controller design results in $k_p = \alpha_c L$, where α_c is the bandwidth of the current controller. The integral gain results in $k_i = \alpha_c R_a$. A lossless converter is assumed, so, consequently $k_i \approx 0$ since $R_a \approx 0$ and the closed loop function results in a simplified expression as:

$$G_c(s) = \frac{\alpha_c}{s + \alpha_c} \quad Y_i(s) = -\frac{s}{L_f (s + \alpha_c)(s + \alpha_f)} \quad (4.7)$$

and the matrix form in the converter dq frame is described as

$$i_{dq} = \begin{bmatrix} g_c(s) & 0 \\ 0 & g_c(s) \end{bmatrix} i_{dq}^* + \begin{bmatrix} y_i(s) & 0 \\ 0 & y_i(s) \end{bmatrix} v_{g,dq} \quad (4.8)$$

The simple structure of the ACC closed loop transfer function allows a design based only on the desired bandwidth. In [22] a bandwidth of $\alpha_c \leq 0.2 \cdot (2\pi f_{sw})$ is recommended and the bandwidth α_f of the low pass filter is suggested to be never larger than $0.1\alpha_c$. Finally, for this VSC application, the selection of the output filter is important since it does not only affect the power quality but also have an impact in the controllers dynamics, as seen from Eq. 4.7. According to [34] a series inductor in each phase is a cost-effective solution with good dynamic performance. In [22], it is stated that $\alpha_c L_f$ should be in the range of 1 p.u. The actual values of the parameters can be found in Table 4.1.

4.1.2 Phase Locked Loop (PLL)

The system has to be synchronised to decouple active and reactive power terms, what enables a better controllability. The PLL is responsible for this task. By tracking voltage amplitude V_m of the grid and the phase angle θ_g , it synchronises the converter dq -frame with the grid dq -frame. The error between the two frames, i.e. the different between the angles $\Delta\theta$, is tracked by the PLL. Considering steady-state conditions the angle variations are really small what allows to linearise at the vicinity of the operating point t and can be described as

$$\epsilon = K \cdot \sin(\theta_g^* - \theta_g) \approx K \cdot (\theta_g^* - \theta_g) = K \cdot \Delta\theta, \quad (4.9)$$

where K is a constant [32, p.54].

During steady state the error is zero and only transients introduce $\epsilon \neq 0$. In this project the input for the PLL is $v_{g,dq}$, i.e. the measured grid voltage transferred in the dq system, and can be described as

$$v_{g,d} = |v_{g,dq}| \cdot \cos(\Delta\theta) \quad (4.10a)$$

$$v_{g,q} = |v_{g,dq}| \cdot \sin(\Delta\theta) \quad (4.10b)$$

The difference of $\Delta\theta$ is zero in steady state, so Eq. 4.10b is zero in normal operation. Thus the value of $v_{g,q}$ can be taken as the input error of the PLL [20].

In this thesis the PLL is implemented as depicted in the Fig. 4.3. If the value of v_q is unequal to zero the PI controller adds or subtracts $\Delta\omega_g = \Delta\dot{\theta}_g$ to the grid frequency $\omega_{g,0}$ in order to align the q -axis. The angular frequency ω_g is integrated to the angle θ_g and fed back to the dq transformation block.

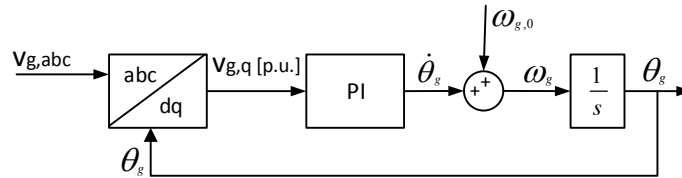


Figure 4.3: PLL control block diagram

With v_g as the grid dq -voltage, the small signal expression of the dq -voltage v_g^c of the converter can be expressed as

$$v_g^c = v_g e^{-\Delta\theta} \rightarrow v_g^c = \Delta v_g - j v_{g,0} \Delta\theta \quad (4.11)$$

The superscript c represents the converter dq -frame, whereas the subscript 0 represents the operational point at 33 kV. Taking 4.11 into account, the open-loop transfer function of the system can be defined as

$$\Delta\omega_g = \frac{d}{dt}\Delta\theta = F_{PLL}(s) \cdot \text{Im}\{v_g^c\} = F_{PLL}(s) \cdot (\text{Im}\{\Delta v_g\} - jv_{g,0}\Delta\theta) \quad (4.12)$$

and the transfer function of the PLL results in

$$G_{PLL}(s) = \frac{\Delta\theta}{\text{Im}\{\Delta v_g\}} = \frac{F_{PLL}(s)}{s + v_{g,0}F_{PLL}(s)}, \quad (4.13)$$

where $F_{PLL}(s) = k_{P,PLL} + k_{I,PLL}/s$.

With the design parameters as in [22], the proportional gain is chosen as $k_{P,PLL} = \alpha_{PLL}/v_{g,0}$ and $k_{I,PLL} = 0$. In [22] two reasons are stated why k_i can be assumed as zero. One function of the integral part is to remove the steady state error of a mismatch between actual and model inductances, which might result in a wrong decoupling of the d and q axes. This is not the case in this study, since the same values are set. The other function is to remove the steady state error due to the voltage drop over the filter resistance, which is not considered.

However, without an integral gain the time domain simulation takes notably longer to reach steady state. It is found that by including a very small integral gain, $k_{i,PLL} = 10e^{-3}$, the properties of the system are not significantly changed with respect to an assessment with $k_{i,PLL} = 0$. In this way, for analysis purposes the transfer function of the PLL can be simplified to 4.14, where α_{PLL} is the bandwidth of the controller.

$$G_{PLL} = \frac{\alpha_{PLL}}{s + \alpha_{PLL}} \cdot \frac{1}{v_{g,0}} \quad (4.14)$$

Inserting Eq. 4.14 in the small signal expression of 4.11 results in a transfer matrix G_{pll}^s between converter and grid voltage as

$$\Delta v_g^c = \underbrace{\begin{bmatrix} 1 & 0 \\ 0 & 1 - v_{g,0}G_{PLL}(s) \end{bmatrix}}_{G_{pll}^s} \begin{bmatrix} \Delta v_{g,d} \\ \Delta v_{g,q} \end{bmatrix} \quad (4.15)$$

Linearising the relation between converter output current in the two synchronous frames $i = e^{j\Delta\theta}i^c$ results in

$$\Delta i = \Delta i^c + i_0\Delta\theta \quad (4.16)$$

The expression of $\Delta\theta$ is substituted with $G_{PLL}(s) \cdot \text{Im}\{\Delta v_g\}$ from Eq. 4.13 . Further on, given that $i_{d,0} = P_{WT}/v_{g,0}$ and $i_{q,0} = -Q_0/v_{g,0}$ the expression be rewritten as

$$\Delta i = \Delta i^C + \underbrace{\begin{bmatrix} 0 & Q_0/V_{g,0}G_{PLL}(s) \\ 0 & P_{WT}/V_{g,0}G_{PLL}(s) \end{bmatrix}}_{G_{pll}^p} \begin{bmatrix} \Delta v_{g,d} \\ \Delta v_{g,q} \end{bmatrix}, \quad (4.17)$$

with G_{pll}^p as transfer function of $\Delta i/\Delta v_g$.

4.1.3 Direct Voltage Control (DVC)

In the 2LC, the DVC keeps the dc voltage v_{dc} across the capacitor within acceptable limits by controlling the stored energy in the capacitor. In steady state the energy E flowing into the capacitor is zero, so from Fig. 4.1 it can be deduced that $P_{WT} = P_{vsc}$ for steady state conditions. Otherwise, an energy exchange ΔE across the capacitor results in $P_{cap} = P_{WT} - P_{vsc}$. The control of the energy E is related to the control of the power exchange between converter and grid [32, 20].

The power flowing into the capacitor is defined in Eq. 4.18 where C is the capacitor of the dc link.

$$\frac{C}{2} \frac{v_{dc}^2}{dt} = P_{WT} - P_{vsc} \quad (4.18)$$

Linearising the expression around the operation point gives

$$\Delta P_{vsc} = \Delta P_{WT} - C \cdot v_{dc}^0 \cdot \frac{d}{dt}(\Delta v_{dc}) \quad (4.19)$$

For generating the correct reference power, which will define i_d^* , the DVC is responsible to keep the voltage difference to zero. To this aim, a PI controller is applied to the error measured in the dc link voltage, as

$$P_{ref} = - \underbrace{\left(k_{p,dc} + \frac{k_{i,dc}}{s} \right)}_{F_{dc}(s)} (v_{dc}^* - v_{dc}) + H_{dc}(s) P_{WT} \quad (4.20)$$

where $H_{dc}(s) = \frac{\alpha_{fd}}{s + \alpha_{fd}}$

Generally the current control loop should be around 10 times faster than outer control loops [32]. Therefore according to the parameters design in [22], the DVC

bandwidth is set to $\alpha_d = 0.1\alpha_C$, which is included in the controller gain $k_{p,dc} = \alpha_d C$ and $k_{i,dc} = 0$. However, for the same reasons given for the PLL, the integral gain is chosen to be small but different than zero ($k_{i,dc} = 10e^{-3}$). The values of the basic design parameters of this controller can be found in Table 4.1 at the end of this section.

Having the ACC loop much faster than the voltage control loop, from the view of the DVC the actual grid currents can be seen as equal to the reference currents. This decouples the inner and outer control loop and it can be assumed as $i_d \approx i_d^*$. By neglecting the converter and filter losses, the injected power in the 2LC at the dc side can be equated with the power flowing into the ac grid, so $P_{vsc} \approx u_{g,d} \cdot i_d \approx u_{g,d} \cdot i_d^*$ [20]. For steady state analysis it can be further assumed that $v_{dc}^* = v_{dc}^0$ and constant P_{WT} , so the linearisation of Eq. 4.20 results in $\Delta P_{ref} = v_{dc}^0 F_{dc}(s) \Delta v_{dc}$.

Applying the small signal to the reference current $i_d^* = P_{ref}/u_{g,d}$ it results in

$$\begin{aligned} \Delta i_d^* &= \frac{\Delta P_{ref}}{v_g^0} - \frac{P_{WT}}{(v_g^0)^2} \cdot H_{dc}(s) \Delta v_{g,d} \\ &= \frac{v_{dc}^0 F_{dc}(s) \Delta v_{dc}}{v_g^0} - \frac{P_{WT}}{(v_g^0)^2} \cdot H_{dc}(s) \Delta v_{g,d} \end{aligned} \quad (4.21)$$

Eq. 4.21 displays the change of the reference d -current depending on the change in grid and dc voltage. Using Eq. 4.8 and the steady-state expressions $i_{d,0} = P_{WT}/v_{g,0}$ and $i_{q,0} = -Q_0/v_{g,0}$, Δv_d can be substituted, resulting in

$$\Delta i_d^* = -G_{dc,d}(s) \Delta v_{g,d} + G_{dc,q}(s) \Delta v_{g,q} \quad (4.22)$$

where

$$G_{dc,d}(s) = \frac{\left[-y_i(s) - \frac{P_{WT}}{v_{g,0}^2} + \frac{P_{WT}}{v_{g,0}^2} g_c(s) H_{dc}(s) \right] F_{dc}(s)}{sC_{dc} + g_c(s) F_{dc}(s)} - \frac{P_{WT} H_{dc}(s)}{v_{g,0}^2} \quad (4.23)$$

$$G_{dc,q}(s) = \frac{-Q_0 F(s)}{v_{g,0}^2 [sC_{dc} + g_c(s) F_{dc}(s)]} \quad (4.24)$$

Assuming that the reactive power is controlled to zero, $Q_0 = 0$, then $G_{dc,q}(s) = 0$, so

$$\Delta i^* = \underbrace{\begin{bmatrix} G_{dc,d}(s) & 0 \\ 0 & 0 \end{bmatrix}}_{G_{dc}} \Delta v_g \quad (4.25)$$

For a graphical explanation the control scheme is displayed in Fig. 4.4.

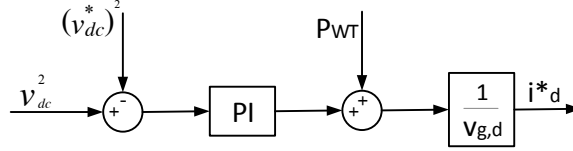


Figure 4.4: Direct Voltage controller block

It can be observed that the DVC has only an impact on the d component of the reference current.

4.2 MMC - HVDC Station

As described in [35], the offshore station of the HVDC system modelled in this project controls the frequency, magnitude and phase angle of the voltage at the IP. The dc-link voltage of the HVDC system is assumed to be stable and controlled by the grid side converter. Therefore the MMC operation should correct any disturbance coming from the offshore wind farm network in order to keep a constant voltage across the IP capacitors. To this aim a cascade controller structure is implemented including a current control loop and an alternate voltage control as the one showed in Fig. 4.5. According to [7] the same controllers structures used for a conventional VSC-HVDC station can be applied in the MMC. It can be seen in the figure, that the current flow direction is defined as in the 2LC, i.e. i_t is flowing out of the converter. The alternate voltage control has the measured grid quantities, the reference voltage magnitude and a reference angle as input. The generated currents i_{dq}^* is the reference for the current controller which sends out a reference voltage for the switching operation. For a clearer appearance only one phase of the MMC is displayed, which includes in series connected submodules (SM). The inductances and resistances are equal as $L_{up} = L_{lw}$ and $R_{up} = R_{lw}$. It is assumed that the circulating currents have no effect on the ac side of the converter

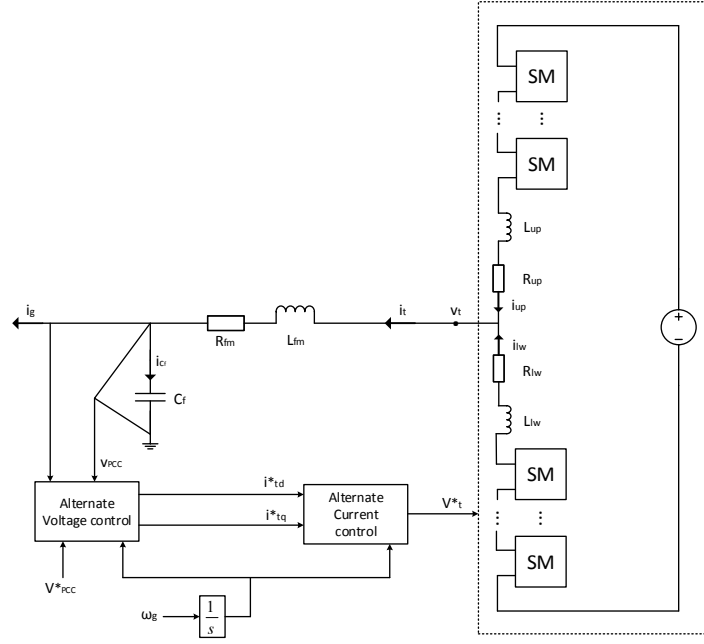


Figure 4.5: MMC model and control structure

[36], and hence have no relevance for the stability analysis proposed in this project. For further reading about MMC it is referred to [3, 6, 37, 38].

4.2.1 Alternate Current Control (ACC)

Similar to the ACC designed for the WT-2LC, the current control strategy is based on the dynamics in the grid given by the current i_t flowing between the IP and the MMC terminals, as represented in Fig. 4.5. The ac dynamics are given by

$$v_t = v_{IP} + j\omega_g L_{fm} i_t + R_{fm} i_t + \frac{di_t}{dt} L_{fm} \quad (4.26)$$

Where v_t is the the voltage at the MMC terminals, v_{IP} is the voltage across the IP capacitor, and L_f and R_f are the MMC filter inductance and resistor respectively which are determined by the following parameters

$$L_{fm} = L_t + \frac{L_{up}}{2} \quad R_{fm} = R_t + \frac{R_{up}}{2} \quad (4.27)$$

The implemented current control algorithm is given by the following expression in Laplace form in the dq -rotating reference frame

$$v_{t,dq}^* = G_{ac} \cdot (i_{t,dq}^* - i_{t,dq}) + (j\omega_g L_{fm} - R_{gc}) \cdot i_{t,dq} + H_{ac} \cdot v_{IP,dq} \quad (4.28)$$

Where

$$G_{ac}(s) = \left(k_{pc} + \frac{k_{ic}}{s} \right) \quad H_{ac}(s) = \left(\frac{\alpha_{fm}}{\alpha_{fm} + s} \right) \quad (4.29)$$

This strategy is based on the current control given in [22]. In this way, the MMC current control loop has a similar structure to the one derived in Fig 4.2 for the WT-VSC. However, in this case a term for active damping R_{gc} is also added in order to increase the robustness of the MMC controller against disturbances.

Following the same procedure, by equating Eq. 4.26 with Eq. 4.28 and assuming no delay time $T_d = 0$, the following expression is obtained

$$i_{t,dq} = G_{cm}(s) i_{t,dq}^* + Y_{im}(s) v_{IP,dq} \quad (4.30)$$

Where $G_{cm}(s)$ and $Y_{im}(s)$ are the closed-loop transfer function and the admittance of the MMC respectively and are defined as

$$G_{cm}(s) = \frac{k_{pc}s + k_{ic}}{L_{fm}s^2 + R_{fm}s + R_{gc}s + k_{pc}s + k_{ic}}, \quad (4.31)$$

$$Y(s) = -\frac{s^2}{(L_{fm}s^2 + R_{fm}s + R_{gc}s + k_{pc}s + k_{ic})(s + \alpha_{fm})} \quad (4.32)$$

resulting in the dq space-vector expression given by Eq.4.33 similar to the one found for the WT-VSC in

$$i_{t,dq} = \begin{bmatrix} g_{cm}(s) & 0 \\ 0 & g_{cm}(s) \end{bmatrix} i_{t,dq}^* + \begin{bmatrix} y_{im}(s) & 0 \\ 0 & y_{im}(s) \end{bmatrix} v_{IP,dq} \quad (4.33)$$

Setting a current control bandwidth $\alpha_{cm} \leq 0.2\omega_{sw}$ as suggested in [22], the virtual resistor can be defined as a function of the inductance of the system $R_{gc} = 0.1\alpha_{cm}L_{fm}$. Hence the parameters of the PI controller are $k_{pc} = \alpha_{cm}L_{fm}$ and $k_{ic} = \alpha_{cm}(R_{fm} + R_{gc})$, retaining the current controller bandwidth of the closed-loop transfer function $G_{cm}(s)$. According to what stated in [22], L_{fm} is designed to keep $\alpha_{cm}L_{fm}$ in the range of 1 p.u. Finally, the bandwidth of the feed-forward low pass filter is selected as $\alpha_{fm} = 0.1\alpha_{cm}$. The values of the basic design parameters are given in Table 4.1.

By including an integration gain in the controller structure the system reaches faster steady state conditions. This is an important feature for the time domain simulations, since as it will be further explained in section 5.2, the MMC should set the voltage at the IP during the connection of the different parts of the OWF.

4.2.1.1 Alternate Voltage Control (AVC)

The relation between the IP voltage v_{IP} and the current in the terminals of the MMC i_t , and the grid current i_g can be written as

$$i_{Cf} = C_f \frac{dv_{IP}}{dt} + j\omega_g C_f v_{IP} = i_t - i_g \quad (4.34)$$

what can be derived from Fig. 4.5.

Eq. 4.34 captures the dynamics of the voltage across the capacitor C_f giving the basis for the design of the voltage control. The reference value of the network voltage v_{IP} is a constant value imposed in the voltage controller. In a similar way, the reference frequency is set in the controller by the integration of the angular frequency ω_g , as suggested in [35]. The controller scheme for the AVC is presented in Fig. 4.6.

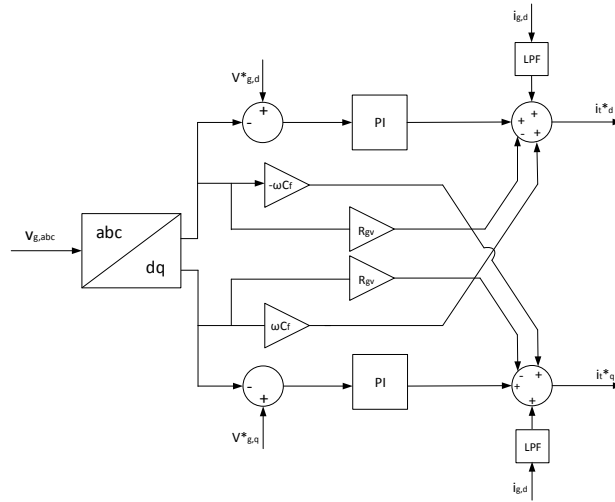


Figure 4.6: Alternate Voltage Controller AVC implemented in the MMC

The voltage control sets the reference current at the terminals of the MMC $i_{t,dq}^*$ sent to the current controller. Eq. 4.35 represents the alternate voltage control strategy implemented in this project which is based on [35]

$$i_{t,dq}^* = G_{vc} \cdot (v_{IP,dq}^* - v_{IP,dq}) + (j\omega_g C_f - R_{gv}) \cdot v_{IP,dq} + H_{vc} \cdot i_{g,dq} \quad (4.35)$$

Where

$$G_{vc}(s) = \left(k_{pv} + \frac{k_{iv}}{s} \right), \quad H_{vc}(s) = \left(\frac{\alpha_{fv}}{\alpha_{fv} + s} \right)$$

A PI controller is applied to the error term of the IP voltage and the grid current $i_{g,dq}$ is fed-forward through a low pass filter in order to get rid of high frequency disturbances. A decoupling term is included in the control process enabling independent control of v_{IP}^d and v_{IP}^q . In a similar way as in the current controller loop, a virtual resistor R_{gv} is also introduced to increase the robustness of the system and at the same time help finding a proper value for the integrator term in the controller. The bandwidth of the AVC for the MMC is set to $\alpha_{vm} = 0.3\alpha_{cm}$ seeking for a fast response in the time-domain simulation. With an active damping term $R_{gv} = \alpha_{vm}C_f$, the values of the PI parameters are defined as $k_{pv} = \alpha_{vm}C_f$ and $k_{iv} = \alpha_{vm}^2 C_f$. The low-pass-filter bandwidth is set $\alpha_{vm} = \alpha_{fv}$. The selection of the IP capacitor C_f takes into account the need for reactive power support in the OWF network, assuming the aggregated π -model of the transmission system described in the next section.

The small signal expression of Eq. 4.35 is derived in Eq. 4.36.

$$\Delta i_{t,dq}^* = \frac{(j\omega_g C_f s - R_{gv} s - k_{pv} s - k_{iv})}{s} \Delta v_{IP,dq} + \left(\frac{\alpha_{fv}}{\alpha_{fv} + s} \right) \Delta i_{g,dq} \quad (4.36)$$

Table 4.1: Summary of the design parameters of both converters

MMC		2LC	
Vb	132kV	Vb	33 kV
$f_{sw,m}$	900 Hz	f_{sw}	1950 Hz
L_{fm}	$L_t = 62 \text{ mH}$	L_f	3.9 mH
	$L_{up} = R_{lw} = 6.2 \text{ mH}$	C	250 μF
R_{fm}	$R_t = 2 \Omega$	ACC	$\alpha_c = 1253.5 \text{ rad/s}$
	$R_{up} = R_{lw} = 0.2 \Omega$		$\alpha_f = 125.3 \text{ rad/s}$
C_f	9 μF	DVC	$\alpha_d = 125.3 \text{ rad/s}$
ACC	$\alpha_{cm} = 1131 \text{ rad/s}$		$\alpha_{fd} = 125.3 \text{ rad/s}$
	$\alpha_{fm} = 113.1 \text{ rad/s}$	PLL	$\alpha_{PLL} = 31.4 \text{ rad/s}$
AVC	$\alpha_{vm} = 339.3 \text{ rad/s}$	P_{wt}	180 MW
	$\alpha_{fv} = 339.3 \text{ rad/s}$	Q_0	0 MW

In table 4.1 the design parameters of the two converters are presented. The bandwidth of the controllers are obtained base on the recommendations given in [22]. The inductances of the respective filter are then obtained for keeping $\alpha_c L$ in the range of 1 p.u as suggested in [10]. In the MMC case, the rest of the filtering elements are designed around this inductance value.

4.3 AC System

In Section 3.1 a single line diagram of the OWF was presented. In Fig. 3.2, it can be seen that the ac system collection and transport system can be divided up in three sections: OWF ac network or collection grid, the offshore substation, and the export cable.

4.3.1 Collection grid

The collection grid is assumed to be comprised by 6 arrays with 6 WTs connected to each of them. According to [39], a π -circuit model with lumped parameters is a suitable representation for cables under 30 km length. Similar stability studies have been performed in [20], using the same representation of the cable system.

The designe of the cables is based on the current that they are assumed to carry. According to [40], the minimum current carrying capacity for each cable can be calculated as

$$I_{rat,min} = \frac{S_{n,WT}}{\sqrt{3} \cdot U_{n,min}} \cdot 150\% \quad (4.37)$$

where $S_{n,WT}$ is the rated power injected by the wind turbines and it can be assumed that $S_{n,WT} = P_{n,WT}$. The voltage $U_{n,min}$ is calculated as $0.9 \cdot 33 kV$, which is the minimum operating voltage. Due to safety reasons, cables are over-dimensioned so 50% of the capacity is added to the minimum current calculation [40]. The user's guide of ABB [1] includes a range of different XLPE submarine cables, which data is used for designing the collection grid cables. In the 6 different arrays, the cable cross section is varying and chosen based on [1, Table 33]. The parameter of the different cables can be seen in table 4.2 and are taken from [1, Table 43]. Branch '1' is the cable connecting the array with the the step up transformer and the branch '6' is the cable furthest out.

It can be considered as a general rule that in wind farms, WTs are spaced 5-9 rotor diameters apart in the predominant wind direction, and 3-5 diameters perpendicular to the wind direction [41]. Taking as reference the diameter of the Gamesa G128-5.0 MW WT, with a diameter of 128m [42], the length of the array cables are calculated.

Table 4.2: Cable data for each array branch and the aggregated total impedance of all 6 arrays [1].

Cable branch	R [$m\Omega$]	C [μF]	L [mH]
6	177	0.18	0.44
5	177	0.18	0.44
4	70	0.24	0.38
3	42	0.29	0.35
2	21	0.38	0.31
1	16.8	0.41	0.3
Total impedance	439	0.184	0.22

The parameters of the collection grid can be aggregated for each array by

$$R_{array,k} = \sum_{i=1}^6 R_i \cdot l_i, \quad C_{array} = \sum_{i=1}^6 C_i \cdot l_i, \quad L_{array} = \sum_{i=1}^6 L_i \cdot l_i \quad (4.38)$$

and finally expressed as

$$R_{co} = \frac{1}{\sum \frac{1}{R_{array,k}}}, \quad C_{co} = \frac{1}{\sum \frac{1}{C_{array,k}}}, \quad L_{co} = \frac{1}{\sum \frac{1}{L_{array,k}}} \quad (4.39)$$

for the whole collection grid [27]. Subscript i determines the individual branches and l_i is the length of the specific cable branch. k determines the number of the array. The total collection grid values are presented in table 4.2 as well.

4.3.2 Transformer

The transformer steps up the 33kV to the 132kV, which is also the voltage level of the DC system. The main parameters for the step-up transformer are presented in table 4.3. Note, that the system is composed of two transformers connected in parallel. Thus load losses and rated power level is doubled compared to the values presented in the table. They are represented as a single transformer like mentioned

and modelled in the Chapter of system characterisation (3.1) and the values are simply calculated for a transformer with double the power level, so 240 MVA.

The rated current is hereby calculated as

$$I_1 = \frac{S}{\sqrt{3}V_n} = 4200 A \quad (4.40)$$

From the given load losses the resistance of the transformer can be obtained as:

$$R_{01} = \frac{W_{Loss}}{I_1^2} = 0.039 \Omega \quad (4.41)$$

With the short circuit impedance calculated for one transformer as $Z_{SC} = \frac{0.1 \cdot U_{n,HV}}{I_1}$ the impedance and the inductance results in

$$X_{01} = \sqrt{Z_{SC}^2 - R_{01}^2} = 3.14 \Omega, \quad L = \frac{X_{01}}{2\pi 50} = 0.02 H \quad (4.42)$$

Table 4.3: Left - Parameter of one single transformer. Right - Resulting parameter for parallel connection

Rated Power level	120 MVA	Modelled transformer	
Voltage step ($U_{N,HV}/U_{N,LV}$)	132/33 kV	Rated Power level	240 MVA
Load Losses W_{Loss}	345 kW	L_{trafo}	0.01 H
short circuit impedance Z_{sc}	10 %	R_{trafo}	0.039 Ω

In the grid system the transformer will therefore modelled as the inductance L_{trafo} and the resistance R_{trafo} .

4.4 Summary

This chapter describes the careful design of the three subsystems, 2LC, ac network and MMC which are comprised in the OWF network. The converters are designed independently. Controllers which are implemented in the converters differ between the MMC and the 2LC what consequently results in different linearised analytical expressions describing their operation. The dynamic relations of the 2LC are slightly more complex compared to the MMC, since this converter implied two outer control loops, which influence the IAM unequally. The implemented control structures of the MMC influence d and q entries equally, giving the IAM a more symmetrical

appearance. The ac grid is divided in collection system, transformer and an export cable. The values of the parameters which characterise those components are taken from public data sheets. In the end, each of the three subsystems are described by mathematical expressions including dynamical behaviours. An aggregation to a transfer function or IAM for ac system, MMC and 2LC can be found in the next Chapter.

5 System Implementation

This chapter is dedicated to the implementation of the models that will allow the assessment of the CI between the converters in the analysed closed-loop system. In this way, an analytical model of the individual subsystems is derived based on the mathematical relations given in Chapter 4. Firstly the transfer function and the input admittance matrix of the 2LC is derived and combined with the aggregated π -model of the transmission network to obtain the equations corresponding with $Z_{ac-system}(s)$ in Fig. 3.3. The transfer function of the MMC and its IAM are derived for obtaining the $Y_{MMC}(s)$ subsystem. Also the verification procedure of the mathematical model is stated and modifications when implementing the model in the simulation program PLECS are highlighted.

5.1 Analytical Model

According to the theory presented in Chapter 2, the OWF studied in this project can be built based on the impedance/admittance matrices of the different elements in the system. The input admittance matrices of these elements in the system are obtained by the linearised models of the controllers ruling the operation of the WT-2LC and the MMC. In order to perform stability analysis, the system has to be represented by an impedance and an admittance in order to obtain loop characteristics. In Fig. 5.1 it is illustrated clearly how the model is split into an ac system impedance and an MMC admittance. The ac system impedance includes the WT-2LC with its filters and the cable system. (Merely for a clearer appearance in the figure, the ac grid is represented by one single π -model.) The IAM of the MMC includes only the converter and its filters. The red marked voltage v_{IP} and current i_g define the point of connection from which the individual transfer functions are seen.

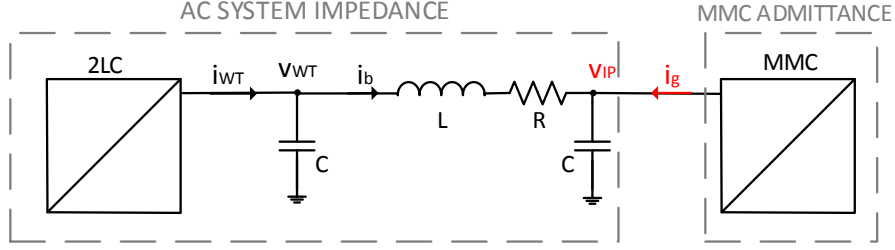


Figure 5.1: System represented by combined impedance (2LC and ac grid) and admittance (MMC)

5.1.1 AC system impedance

The impedance of the ac system contains the 2L-VSC, the collection grid, transformer and the export cable, whereas cables are represented in a π -model. The 2LC can be either represented by its IAM or its transfer function. The IAM is useful for studying the impact of the individual controller parameter, as it is stated in [22] and will be demonstrated in the analyses of this study. The transfer function can be used for study its stability and further on it is connected with the cable system to obtain the ac system transfer function.

For simplification the IAM and the admittance transfer function of the 2LC in itself is obtained before deriving the ac-system impedance.

IAM of the 2L-VSC

The design approach in the previous section is based on the study of the input admittance matrix for a VSC at the onshore side of an HVDC system, which was derived in [22]. Unlike in the mentioned paper, in the case of a the grid side converter the current is flowing from the DC side to the ac side. Consequently the current is defined as outflowing from the converter (also visible in Fig. 5.1 referring to i_{WT}). The approach of obtaining the IAM is overtaken from the mentioned paper. The final matrix is defined by the controllers ACC, PLL and DVC.

Combining equations 4.8, 4.25, 4.15 and 4.17 to a linearised system as

$$Y_{2LC}^m(s) = Y_i(s)G_{pll}^{s}(s) + G_c(s)G_{dc}(s) + G_{pll}^p(s) \quad (5.1)$$

results in the IAM of the 2LC

$$Y_{2LC}^m(s) = \frac{\Delta i_{WT,dq}}{\Delta v_{WT,dq}} \quad (5.2)$$

with its components as

$$\begin{aligned} Y_{2LC,dd} &= y_i + G_c \cdot G_{dc,q} & Y_{2LC,dq} &= 0 \\ Y_{2LC,qd} &= 0 & Y_{2LC,qq} &= y_i(1 - G_{pll} \cdot V_{g,0}) + \frac{P_{wt}}{V_{g,0}} \cdot G_{pll} \end{aligned} \quad (5.3)$$

The matrix is helpful if the influences of the controller parameters are of interest, so these matrix entries can be examine in more detail. This is of particular importance, if the system is unstable or non-passive and the origin of the instability wants to be studied.

The IAM can be also expressed as transfer function by

$$Y_s(s) = \frac{1}{2} [Y_{dd}(s) + Y_{qq}(s) + j(Y_{qd}(s) - Y_{dq}(s))], \quad (5.4)$$

where Y_s is the equivalent admittance per phase ([43]). In the case of the admittance of the 2L-WT the imaginary parts are zero, so the equivalent transfer function results in:

$$Y_{2LC}(s) = 0.5(Y_{2LC,dd}(s) + Y_{2LC,qq}(s)) \quad (5.5)$$

It is important to mention that this transfer function is obtained from the controllers designed in the dq frame. Consequently when moving to the time domain the frequencies have to be shifted by 50 Hz in order to present the results in the 3 phase system. This is explained more detailed in section 5.3

Total ac-system impedance

The total admittance transfer function is composed of the 2LC controller including its filter inductance and the cable system. By adding the grid system to the already derived admittance $Y_{2LC}(s)$, there are two things which have to be observed:

- The admittance $Y_{2LC}(s)$ is represented in the dq frame so in order to add the cables, the grid dynamics have to be moved to the dq -frame as well.
- In order to compare the transfer functions in the analyses they have to be presented in p.u. However, the collection grid and the export cable are operating at different voltage levels and are connected with a step up transformer, so the cables can not be aggregated by simply adding the components. The low voltage side has to be lumped first, transformed to the high voltage side and then combined with the export cable.

This procedure is done as follows:

1. The low voltage side is aggregated to one impedance Z_2 by combining the 2LC transfer function with the components of the collection grid.
2. This impedance is then transformed to the primary side of the transformer and represented as the admittance Y_1 .
3. The lumped admittance can be implement as it is shown in Fig 5.2 on the high voltage side.

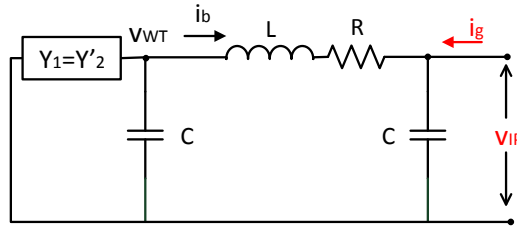


Figure 5.2: Impedance of the ac-system

The final impedance of the ac system is defined as $Z_{ACsys} = \frac{\Delta v_{IP}}{\Delta i_g}$. The grid current sent out from the MMC is the input in the impedance system and the change in the voltage v_{IP} the output. To obtain the transfer function or the impedance Z_{ACsys} the dynamics of the voltages v_{WT} and v_{IP} and the current i_b are defined in the following equations. For moving capacitances and inductances to the dq -frame the

cross coupling term jw_g has to be added. This is realised in the following equations where s^{dq} stands for $s + j\omega_g$. Additionally the derived admittance Y_1 has to be taken into account as well.

$$C \frac{dv_{WT}}{dt} = i_{WT} - i_b s^{dq} C v_{WT} = i_{WT} - i_b \quad (5.6a)$$

$$C \frac{dv_c}{dt} = i_b + i_g s^{dq} C v_c = i_b + i_g \quad (5.6b)$$

$$L \frac{di_b}{dt} + R i_b = v_{WT} - v_c (s^{dq} L + R) i_b = v_{WT} - v_c \quad (5.6c)$$

$$i_{WT} = Y_1 \cdot e_{WT} \quad (5.6d)$$

Combining, rearranging and solving the equations results in the current i_b :

$$i_b = v_{IP} \cdot \frac{Y_1 - s^{dq} C}{\underbrace{1 - (Y_1 - s^{dq} C)(s^{dq} L + R)}_{G_{ib}}} \quad (5.7)$$

Inserting Eq. 5.7 into Eq. 5.6b leads to following expression for the ac system impedance:

$$Z_{ac-sys} = \frac{\Delta v_{IP,dq}}{\Delta i_{g,dq}} = \frac{1}{s^{dq} C - G_{ib}} \quad (5.8)$$

Regarding to the initial Fig. 5.1 it can be summarised that the left block is represented by impedance Z_{ACsys} with a small signal current Δi_g as input and a small signal voltage Δv_{IP} as output. This voltage is the feedback and creates together with the reference voltage v_{IP}^* the input for the MMC admittance, which is derived in the next section.

5.1.2 MMC IAM

As previously stated, the IAM of an MMC is not available in the public domain. Based on the theory given in the previous C, it is deduced that the MMC IAM can be found by following the same procedure as for the WT-2LC where the obtained IAM is shaped by the controllers that rule the operation of the converter. For the purpose of the study in this project, the IAM of the MMC should be calculated at the IP of the HVDC station with the OWF. In section 4.2, it was shown that for the operation of the MMC in the HVDC system, the model can be reduced to two control loops, the inner current control loop and an AVC.

As derived in section 4.2, the AVC generates a reference current which small signal representation is expressed in Eq. 4.36. This reference current is inserted in $\Delta i_{t,dq} = G_{cm}(s) \cdot \Delta i_{t,dq}^* + Y_{mc}(s) \Delta v_{IP,dq}$ (Eq. 4.30). Since the IAM of the MMC should be obtained based on the grid current i_g , then $\Delta i_{t,dq}$ can be substituted by $\Delta i_{g,dq}$ using Eq. 4.34 ($i_{Cf} = C_f \frac{dv_{IP}}{dt} + j\omega_g C_f v_{IP} = i_t - i_g$). In this way, the IAM of the MMC is derived as:

$$Y_{MMC}^m(s) = \frac{\Delta i_{g,dq}}{\Delta v_{IP,dq}} \quad (5.9)$$

The entries in $Y_{MMC}^m(s)$ are obtained by taking the real and imaginary parts of Eq. 5.9, so that $Y_{MMC,dd} = Y_{MMC,qq} = \text{Re}(Y_{MC})$ and $Y_{MMC,dq} = -Y_{MMC,qd} = \text{Im}(Y_{MMC})$. The matrix entries are resulting in:

$$\begin{aligned} Y_{MMC,dd}^m &= -\frac{C_f s + R_{gv} G_{cm} + G_{vc} G_{cm} - Y_{im}}{-H_{vc} G_{cm} + 1} & Y_{MMC,dq}^m &= -\frac{C_f \omega (G_{cm} - 1)}{-H_{vc} G_{cm} + 1} \\ Y_{MMC,qd}^m &= \frac{C_f \omega (G_{cm} - 1)}{-H_{vc} G_{cm} + 1} & Y_{MMC,qq}^m &= -\frac{C_f s + R_{gv} G_{cm} + G_{vc} G_{cm} - Y_{im}}{-H_{vc} G_{cm} + 1} \end{aligned} \quad (5.10)$$

Having a look back to Fig. 5.1 it can be stated now that also the right part is derived. The admittance of the MMC has the voltage error $v_{IP}^* - \Delta v_{IP}$ as input and the grid current change Δi_g as output signal.

To follow the same structure as previously with the 2LC, also the transfer function of the MMC is required. $Y_{MMC}(s)$ is simply

$$Y_{MMC}(s) = Y_{MMC,dd}^m(s) + jY_{MMC,dq}^m(s) \quad (5.11)$$

and will be later implemented in the open loop function to study the total system stability.

5.2 Time Domain Model

To confirm the effectiveness of the approach in the assessment of CI between the VSCs in the studied network a verification of the impedance-based models obtained in subsections 5.1.1 and 5.1.2 is needed. At the same time, it is interesting to have a time domain model in which the effects of the possible CI over the evaluated network can be observed.

The PLECS model is meant to represent the elements of the network in the most realistic form in steady-state conditions, but at the same time it should include the simplifications assumed for the mathematical models.

In the following subsections a description of how the different elements of the network are implemented in PLECS is given.

5.2.1 WT-2LC

The mathematical relations describing the operation of the converters are implemented in PLECS as block systems, which contain the controller structures described in section 4.1. The control is implemented by sending switching signals to the converter switches. This module is a predefined PLECS block that simulated the behaviour of an ideal three-phase 2-level converter which can be controlled by PWM and where no switching delays are included. The dc side of the converter is modelled as a capacitor in parallel with a controlled current source which ramps up the power as soon as the rest of the system is in steady state.

5.2.2 MMC-HVDC

As it is stated in MMC controller design section 4.2, integral gains are important in the controller design. This is considered due to the fact that, in time domain simulations, the MMC sees the transients originated from the connection of the different parts of the network. Considering this fact, the MMC system should reach

steady state conditions as soon as possible to allow further analyses in the system within an short simulation time .

The MMC is built with 10 IGBT-based half bridge cells series connected in each arm. Similar to the model described in [7], for studying interactions between an MMC and ac power systems, the MMC sub-modules are defined with an average configuration. In this way, the dc-side of the cell is modelled as a current source and the switching states of the IGBTs are represented with a controlled voltage source. The voltage sources are then controlled by a phase disposition PWM (PD-PWM) strategy and a sorting algorithm selecting the insertion of the cells as in [36].

5.2.3 Total OWF ac network

In the PLECS model, as done in the mathematical model, the OWF ac network and the export cable are represented with an equivalent π -model. The offshore substation is modelled in accordance to the transformer data given in subsection 4.3.2 with a delta-star transformer block predefined in PLECS.

Firstly, The two converter models are built and studied independently to ensure that the individuals system reaching a steady state operation. It has to be assured that the voltages and currents are in accordance with the expected values before combining the systems.

The PLECS model was built in the first place to verify the mathematical expressions as matrices and transfer functions. Additionally it can verify instability conclusions, which are drawn based on the analytical model.

5.3 System Verification

In order to verify the obtained transfer functions or the 2L-VSC (Eq. 5.5) and the MMC (Eq. 5.9) a frequency sweep is performed over the two controller subsystems, leaving out the ac grid. Firstly the correlation between dq and abc representation will be explained and then the procedure of the admittance matrix verification is stated, including result plots. In the end a verification of the correct steady state conditions is presented.

5.3.1 Equivalent impedance and admittance in the 3-phase system

For the system verification it is important to notice that the frames in which the the controllers are designed, and in which the simulation model is working are not the same. While the transfer functions and admittance matrices are obtained in the dq -rotating frame, the results of the time-domain simulation will be in the 3 phase abc -system. To overcome this problem the transfer functions of the two converters are shifted by $\omega_g = 2\pi 50 \text{ Hz}$ when performing the frequency response.

In [43], a mathematical procedure for obtaining the phase impedances of a system, of which only the dq -based impedances are known, is derived for electric machines. Attention has to be paid to the positive rotation convention and the difference between q or d alignment. In this thesis positive rotation is counter clock wise and the q component is aligned to synchronise the systems. This results in:

$$Y_s(j\omega) = \frac{1}{2} (Y_{dd} [j(\omega - \omega_g)] + Y_{qq} [j(\omega - \omega_g)]) + j\frac{1}{2} [Y_{qd} [j(\omega - \omega_g)] - Y_{dq} [j(\omega - \omega_g)]] \quad (5.12)$$

where Y_s is the equivalent admittance per phase. Applying 5.12 to the obtained frequency sweep of the analytical model allows the direct comparison with the simulation results.

5.3.2 Procedure for verification

PLECS includes a number of analysis tools among which, the ac sweep can be found. Based on small signal responses, the software generates a Bode plot of the system. The first attempts to verify the impedance model of the WT-2LC is done by making use of this implemented tool. However, it is found that the implemented system has to be slightly modified in order to meet the initial condition requirements. This implies for example that the implemented integrator for the PLL had to be exchanged with a C-script in order to avoid an integration to infinity preventing the model of performing a frequency sweep. Moreover, the required simulation time with the available computers is relatively long. When this analysis tool is used for obtaining the MMC frequency response, the analysis can not even be completed due to lack of memory space. As a consequence, a different approach is needed to verify the mathematical models.

The verification method applied in this project is based in the one given in [17], where the characteristic frequency response of the system is obtained for some frequencies of the studied range. Following steps are applied:

1. Inject a small voltage perturbation ($0.05 p.u.$) at a certain frequency at the point from where the admittance model is derived.
2. Wait for the system to reach steady state conditions and measure the current and voltage values in the three phases.
3. From the measured signals, extract the component of the perturbation frequency.
4. Calculate the admittance or impedance of the system at that frequency.

The frequency sweep should be performed considering two things: Firstly, for all evaluated frequencies, the extracted amount of periods should be equal. Secondly, even more important, the time frame in which the measurements are taken should reach from t^0 until $t^0 + n \cdot T_f - 1$. Where, T_f stands for the period of the evaluated frequency f , t^0 should represent the time of the first sample and n the number of periods which are taken. It is crucial that the last sample is not included, since otherwise one point in the cycle is taken twice, what distorts the result. So, since the time period T_f changes with the perturbation frequency, also the observed time frame should change.

5.3.3 Input admittance verification

The verification results for the 2LC and the MMC are plotted in Fig. 5.3 and Fig. 5.4 respectively.

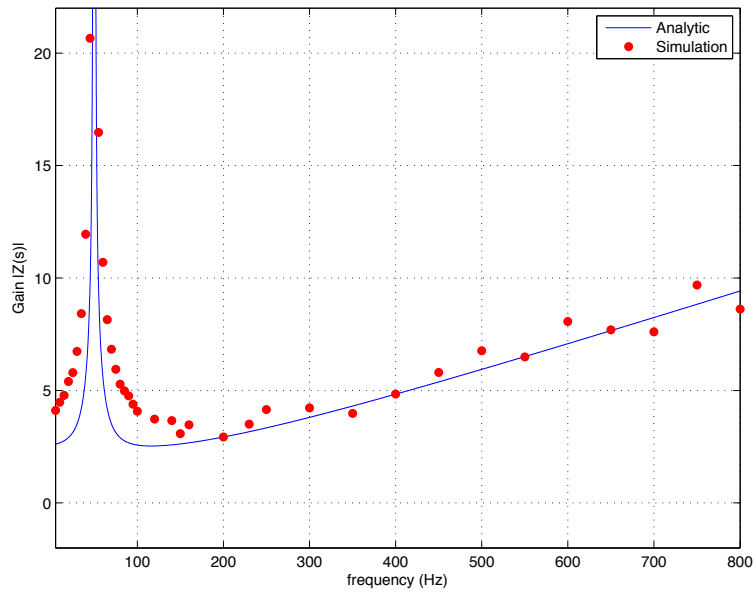


Figure 5.3: Verification of the analytical 2LC IAM means a simulation model

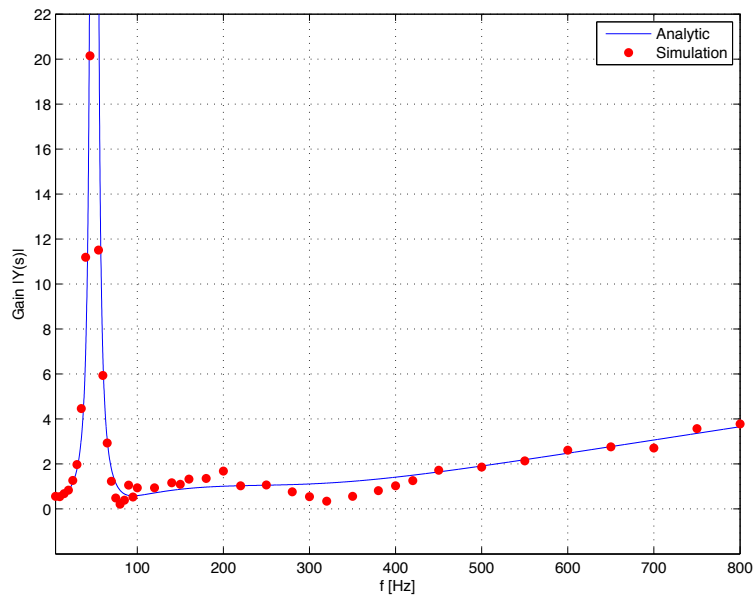


Figure 5.4: Verification of the analytical MMC IAM means a simulation model

Simulation and analytical results follow the same trend but in both cases there

some discrepancy is seen in the lower frequencies around 50 Hz for the 2LC and for the MMC in the higher frequencies. The mismatch is mainly due to the evaluated time frame what was mentioned. The individual time frames are hard to capture correctly when performing the frequency sweep manually. However, and it can be agreed on a verification of the model.

5.3.4 Verification in steady state operation

This section is dedicated to show the steady state conditions of the modelled OWF. The following figures should demonstrate a proper working of the controllers and verify the design earlier described.

The figures show how the different parts of the OWF are step-by-step connected or energised. Switches are implemented in the model to facilitate this sequential connection. For an easier understanding about the location of the switches the single line diagram is added again in Fig. 5.5. The coloured bars in the network show the position of the switches and the time when it is closed.

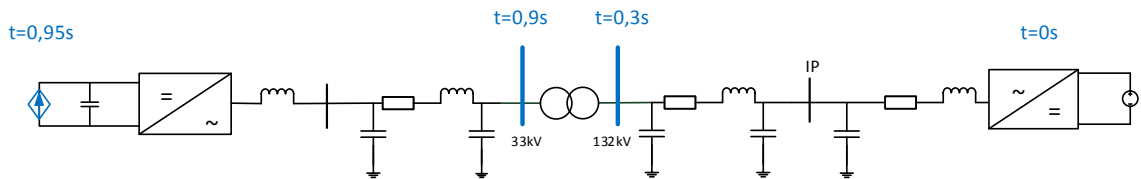


Figure 5.5: Single line diagram showing the switches implemented in the time domain model

Considering the switch operation, the plots in Fig. 5.6 and 5.7 can be divided into 4 different operation steps:

1. Time range: 0-0.3s: Before connecting the transformer and later the wind farm, a constant voltage has to be set at the terminals of the step up transformer. During the first time window the MMC and export cables are in operation until a stable voltage is generated. The peak voltage seen in the Fig. 5.7 measured phase to ground and corresponds with the set reference at $\hat{V} = \frac{\sqrt{2}}{\sqrt{3}} \cdot 132\text{ kV} = 108\text{ kV}$. Further on, a current around 300 A can be noticed in Fig. 5.6 during this time period. This current corresponds to the

reactive current flowing in the system due to MMC filters and the export cable.

2. Time range: 0.3-0.9s: A small change in current can be noticed in Fig. 5.6 during this time period when the step up transformer is connected. Currents become slightly unbalanced due to the connection, but this unbalance is corrected during this time period. For the voltage no change is visible apart from a steady voltage at the defined reference.
3. Time range: 0.9-0.95s: After connecting the rest of the network, i.e. the 2LC a small time frame is given before power is pushed in the system.
4. Time range: 0.95-1.4s: At the time of 0.95 s, the wind farm starts to inject power in the system. The ramp is set to $6000A/s$. After 0.9 ms the power is at its nominal power level of $180 MW$ and the system reaches steady state after the oscillations are reduced. The final current seen in the figure can be calculated as $i = \frac{P}{\sqrt{3} \cdot V_{pk,LO}} = \frac{180e^6}{\sqrt{3} \cdot 107.7kV} = 1113 A$.

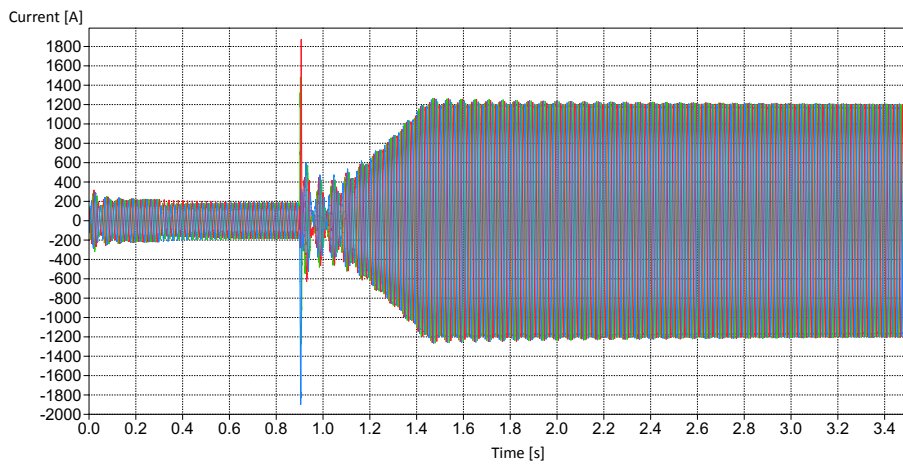


Figure 5.6: 3-Phase Current at the IP

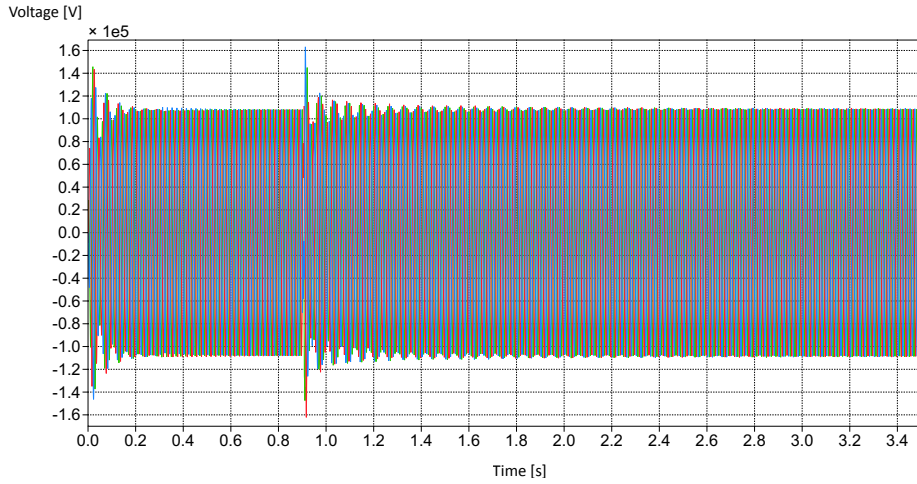


Figure 5.7: 3-Phase Voltage at the IP

The operation of the AVC implemented in the MMC is shown in the Fig. 5.8 and 5.9. Whenever a switch is closed short transients are visible but after some time the reference value is reached again. The dq frame is applied such that the d component results in the magnitude of the voltage and the q component is controlled to zero. Consequently it can be seen in the simulation results that $v_{IP,q}$ is controlled the peak value of the grid voltage $\hat{V} = \frac{\sqrt{2}}{\sqrt{3}} \cdot 132 \text{ kV} = 108 \text{ kV}$, whereas $v_{IP,q}$ is corrected to zero.

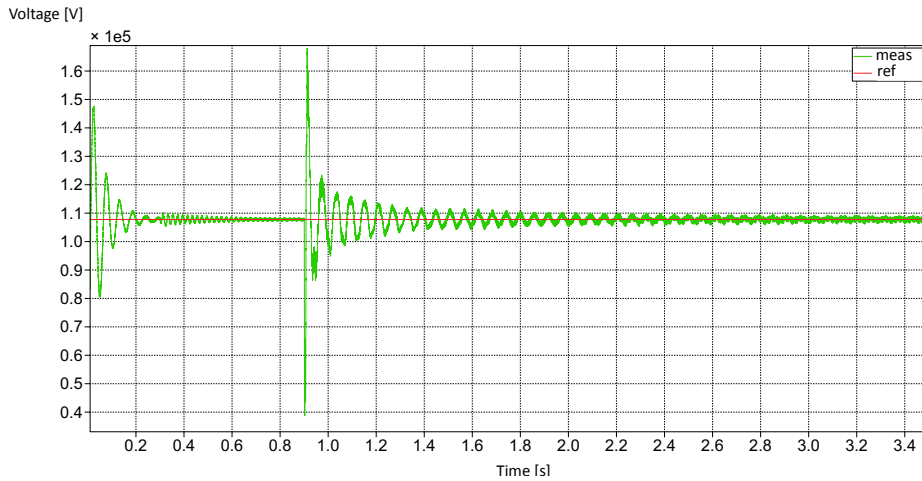


Figure 5.8: Reference and grid voltage v_d at IP

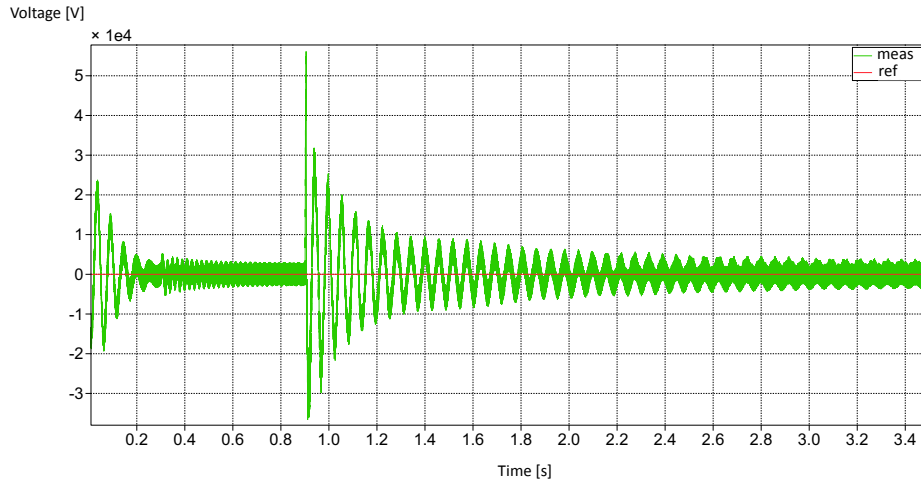


Figure 5.9: Reference and grid voltage v_q at IP

The voltage controller in the MMC generates the reference currents $i_{t,d}^*$ and $i_{t,q}^*$ as an input for the current controller. This reference currents and the actual measured currents at the IP are displayed in Fig. 5.10 and 5.11.

Up to $t = 0.95s$ no active power is flowing in the system, which can be confirmed by the zero d current. However, as it was stated earlier, there is already reactive current flowing in the system due to the MMC filter and the export cable, visible in Fig. 5.11. When power is ramping up active current is starting to flow until it reaches the nominal power output. The current is appearing negative, due to the direction of the measurement device. It is chosen against the natural current flow, because controllers are designed for this sign convention.

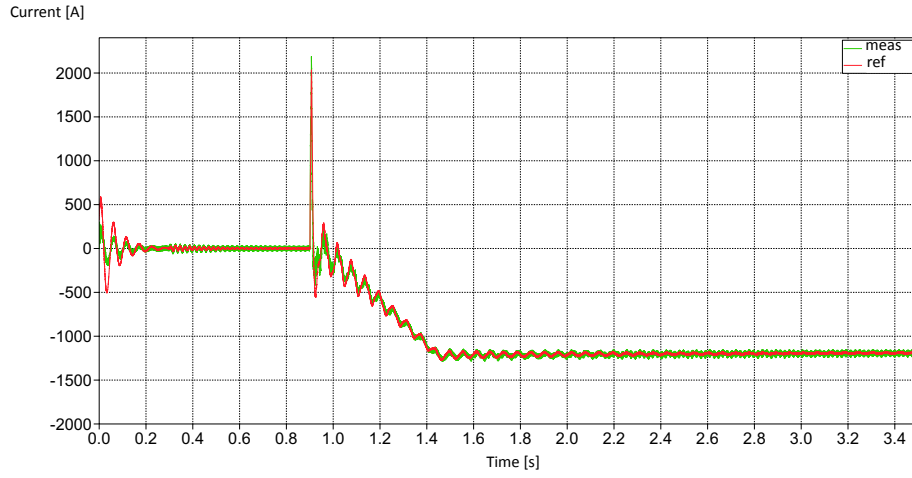


Figure 5.10: Reference and grid current i_d at IP

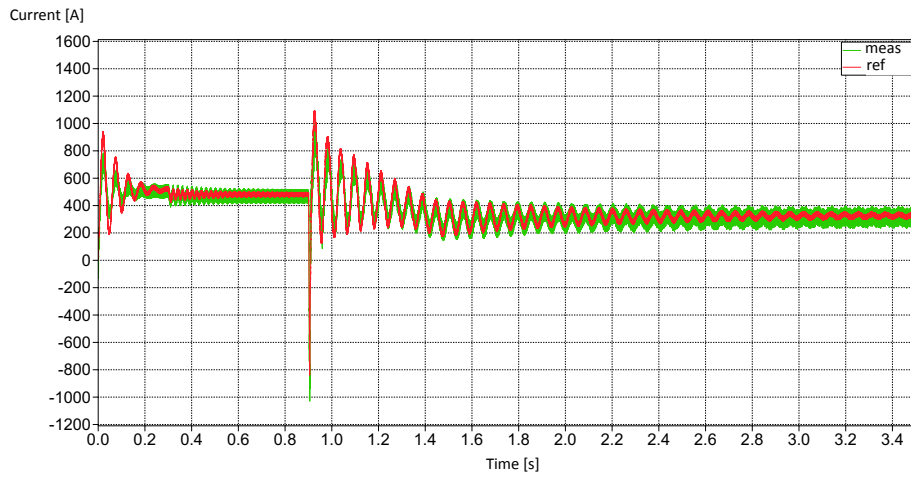


Figure 5.11: Reference and grid current i_q at IP

Since a similar behaviour is seen in the controllers of the 2LC, no further plots are shown.

From the given figures, it can be verified that the system reaches steady state condition and the implemented controllers work for the designed values. This verification allows the later investigation of the stability conditions of the system, derived from the analytical models.

5.4 Summary

In this Chapter all subsystems forming the SISO closed loop are obtained. To this aim, the IAMs of both converters are derived based on the controller structures given in Chapter 4. An effort is done to verify the mathematical frequency-domain models of the converters by a time-domain model, built in PLECS. The frequency response of the IAM of the 2LC and MMC are verified by the trend obtained through an evaluation of the time domain models response under disturbances at same frequencies. For additional verification purposes, reference and actual values of the AAC and AVC implemented in the MMC are plotted, as well as the 3 phase components, measured at the IP. All plots verify that the controllers are operating as expected, oscillations are damped and the system reaches steady state conditions. The 2LC and the MMC IAM blocks are derived in a general manner and can hence be adjusted optionally and implemented in other study cases.

6 Controller Interaction Assessment

In this chapter two analysis tools are presented and in order to determine the possibility of CI in the network, the passivity approach and the net-damping criterion.

First, the impact of the design parameters over the IAM of both converters is evaluated from a passivity perspective. This study only demonstrates how individual controller parameters can influence the passivity of the converters itself. However, no conclusion can be given on the total closed loop system, since the network is not included in this first analysis.

Further on, the total system is studied, by including the OWF transmission network. An attempt to determine the stability of the closed-loop system through the passivity approach is presented. Finally, the net-damping method is used to get a conclusive statement of the total system stability.

6.1 Passivity Analysis of Converter Parameters

Going back to the evaluated problem in the study, it is known that in a system, as the one implemented, can be a risk for CI. This risk is placed by the independent design of each of the converters control parameters. If the converters do not offer enough electrical damping, oscillations at a certain frequency can be sustained or even amplified. The admittance / impedance of the converters is determined by their controllers and physical components. Therefore, it is relevant to analyse the impact that basic design constants have over the passivity of the subsystems. A better understanding about possible non-passive properties of a component can help in the design of other components to obtain a passive operation of the total system. However this knowledge is seldom given in the planning of an OWF [13]. It should be kept in mind, that the OWF transmission system is not yet included, since the aim is to demonstrate the parameter influence on merely the converters.

If an IAM of the component is available it is easier to assess the impact of the individual design parameters through the transfer function of the individual entries. Considering the real part of the individual entries, the influence of the 2LC and MMC can be evaluated for the frequency range of interest $5 - 800 \text{ Hz}$.

In each study it looked at the different matrix entries. It has to be kept in mind that the admittance matrix is comprised as

$$\begin{bmatrix} \Delta i_d \\ \Delta i_q \end{bmatrix} = \begin{bmatrix} Y_{dd} & Y_{dq} \\ Y_{qd} & Y_{qq} \end{bmatrix} \cdot \begin{bmatrix} \Delta u_d \\ \Delta u_q \end{bmatrix}$$

The diagonal elements of the 2LC IAM are zero, so only the diagonal elements Y_{dd} and Y_{qq} are investigated. The elements for the MMC IAM are symmetrical, so $Y_{dd} = Y_{qq}$ and $Y_{dq} = -Y_{qd}$ are studied. Note, in order to analyse the impact on the total admittance Y , the entries can be combined as:

$$Y_s(s) = \frac{1}{2} [Y_{dd}(s) + Y_{qq}(s) + j (Y_{qd}(s) - Y_{dq}(s))].$$

In general a transfer function $Z(s)$ can be defined as *passive* if, and only if the following criteria are true at the same time:

1. $Z(s)$ is stable
2. $\text{Re}[Z(j\omega)] \geq 0$ for $\omega \geq 0$

The 2LC and MMC are stable if all the poles of the individual transfer functions are in the left hand plane. In Fig. 6.1a and 6.1b the poles of the two converters are plotted, showing that a stable system for both converters can be assumed.

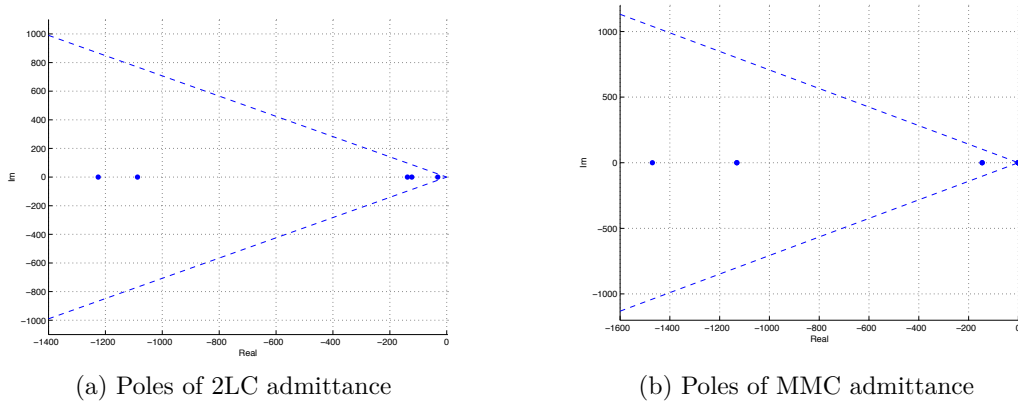


Figure 6.1: Poles of the the converters

Knowing that both transfer functions $Y_{MMC}(s)$ and $Y_{2LC}(s)$ are stable, a conclusion about passivity can be drawn depending on the characteristics of the real parts. Generally it is a valid statement, that the better for the passivity for the systems. It has to be pointed out that since the control of the converters are implemented in the dq -frame, also the following results are presented with respect to that reference frame. Hence, the plotted 0 Hz in the graphs is equivalent to the 50 Hz in the 3 phase abc system.

For the passivity study the IAM of both converters are evaluated when the following parameters are changed:

1. Power level
2. Current controller bandwidth of MMC and 2LC (α_c and α_{cm})
3. Voltage controller bandwidth of MMC and 2LC (α_d and α_{dm})
4. Impact of filtering elements (L_f and C_f)

Note, that in the following plots only the real parts of the matrix entries are shown.

6.1.1 Impact of power level

This subsection is dedicated to study the influence of the power generated by the OWF. The MMC has no power control included and is therefore independent from the operating conditions. Only the WT-2LC is affected by the power level and is discussed in this paragraph.

If only considering the inner control loop (ACC), the WT-2LC would be independent from the power level. However, in this analysis the outer loops are included, and hence the system becomes dependent on the operating conditions. In Fig. 6.2 the real parts of the WT-2LC IAM entries, $Re[Y_{dd}]$ and $Re[Y_{qq}]$, are presented, illustrating the dependency of the 2LC IAM on the power injected from the WT generation unit. On the left plot the whole studied frequency range is plotted, whereas on the right figure a more detailed behaviour of $Re[Y_{qq}]$ at low frequencies is displayed.

Looking at Fig.6.2, it can be said that the system presents non-passivity for every power level in almost the whole frequency range. At lower frequencies the conductance of the converter in $Re[Y_{dd}]$ increases with the power level, reaching a value close to zero in the case of $P_{wt} = 0.1 p.u.$ For $Re[Y_{qq}]$ only in the range of 5-13 Hz a passive behaviour can be identified.

It can be noticed that the power level has almost no influence over $Re[Y_{qq}]$. From the qq matrix entry $[Y_{2LC,qq} = y_i(1 - G_{pll} \cdot V_{g,0}) + \frac{P_{wt}}{V_{g,0}} \cdot G_{pll}]$ it can be seen that the power appears only in the last term $\left(\frac{P_{WT}}{V_{g,0}} \frac{\alpha_p}{s + \alpha_p} \right)$ which is the only term independent of $y_i(s)$. Due to its characteristics, the current control transfer function $y_i(s)$ gets close to zero for small frequencies, which is the region where the power level has a higher impact. From the term it can be also deduced, that in $Re[Y_{qq}]$ the influence of the power starts decreasing after the PLL cross-over frequency (5 Hz). This be noticed in the right plot of Fig. 6.2.

It is worth to mention, that the PLL is responsible for synchronising the dq -frames of converter and grid and it is done by controlling v_q to zero. Consequently the change Δv_q is only visible in Y_{qq} when the converter output voltage is not synchronised with the network voltage.

In general it can be stated that the difference in power level has mainly an influence on the lower frequency range. The active power is more related to the d entry in the matrix and here it can be concluded that at frequencies lower than 80 Hz the passivity is increased with lower power generation.

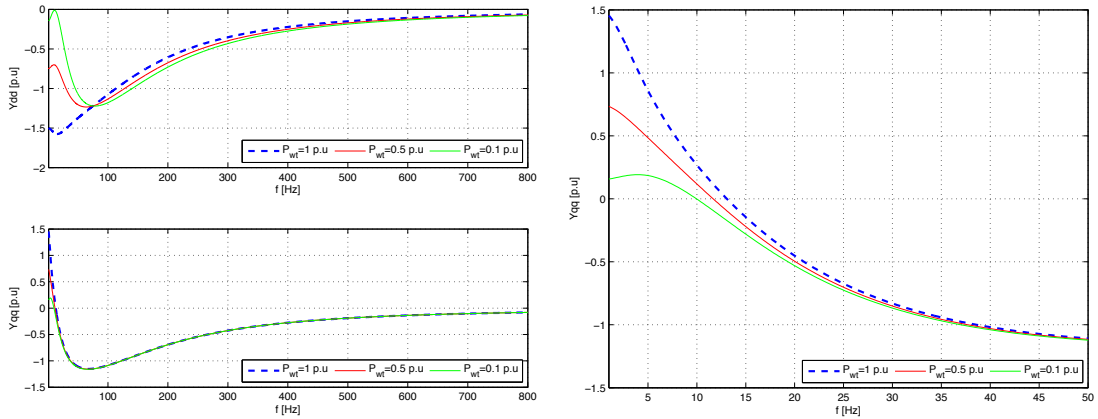


Figure 6.2: Impact of power level on $Re[Y_{qq}]$ and $Re[Y_{dd}]$ of the 2LC. The blue dashed line demonstrates nominal values.

6.1.2 Impact of current controller bandwidth

In this subsection the impact of the current controller bandwidth on the converter passivity is evaluated. The current controller bandwidths are dependent on the switching frequency of the converters. At the same time, the ACC bandwidths, α_c and α_{cm} of the WT-2LC and the MMC respectively, are the reference for the bandwidth design of the outer control loops in each converter; with exception of the PLL. Therefore, by increasing these bandwidths the overall control of the converters becomes faster. If no other parameter is modified, increasing the current controller bandwidths of the systems has different impacts on $Y_{MMC}^m(s)$ and $Y_{2LC}^m(s)$.

The left plot in Fig. 6.3 shows the change of the $Re[Y_{dd}]$ and $Re[Y_{qq}]$ for the WT-2LC with three different current control bandwidths. In the lower range of evaluated frequencies, it can be seen that the faster the ACC the more non-passive the d -entry becomes. On the contrary, in the lower frequencies passivity is increased for Y_{qq} with a faster current control. The impact of a bandwidth change at higher frequencies is negligible. Concluding about the total influence of the current control bandwidth it can be assumed that when adding the two parts together, a faster controller bandwidth has a positive impact on the WT-2LC passivity. This implies that the faster the current control, the smaller is the risk for an instability of the system.

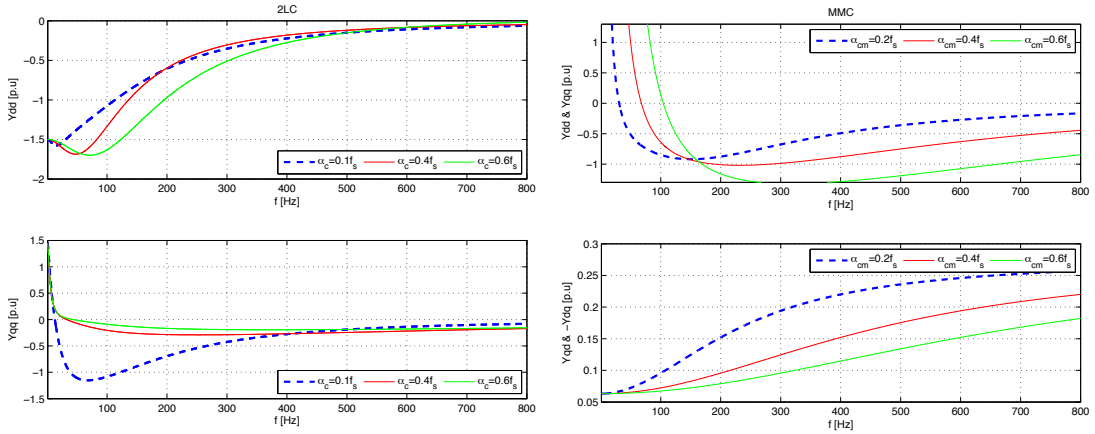


Figure 6.3: Left - Impact of current controller bandwidth on $Re[Y(s)]$ of the 2LC. Right - Impact of current controller bandwidth on $Re[Y(s)]$ of the MMC. The blue dashed line demonstrates nominal values.

The influence of α_{cm} on the MMC is presented in the right plot of Fig. 6.3. Here, increasing the current controller bandwidth has different effects than what was seen for the WT-2LC. For $Re[Y_{dd}]$ & $Re[Y_{qq}]$ below 200 Hz a faster current controller and above a slower current controller is in favour of the passivity. The non-diagonal elements $Re[Y_{qd}]$ and $Re[-Y_{dq}]$ are in general more passive with a smaller bandwidth.

From the plots it can be deduced for whole system $Y_{MMC}(s)$ that for frequencies > 200 Hz passivity is increased for a smaller bandwidths.

6.1.3 Impact of outer loop bandwidths

In this case, the objective is to see how the passivity of the system is affected when the bandwidth of the implemented voltage controller approaches the current controller in both converters.

Note that this implies that the assumption made for the DVC ($i_d \approx i_d^*$) and the AVC ($i_t^* \approx i_t$) will no longer be realistic. Voltage control is the outer control loop, which sets the reference values for the inner control loop, the ACC. Therefore from the inner loop perspective the reference values (i_d^* or i_t^* respectively) should be seen practically constant for a robust and stable control. Mathematically, this means that by increasing the outer control bandwidth the assumption of a constant reference i_d^* or i_t^* is not valid since inner and outer control loops are not properly decoupled anymore. The PI controller is then correcting the error to a reference constantly changing reference, which can compromise the controller system stability. A variation of α_d in the DVC of the 2LC will only involve changes in $Re[Y_{dd}]$. The DVC is controlling the active power, which is only dependent on v_d and i_d . The left plot in Fig. 6.4 shows that the 2LC conductance decreases with the increase of α_d for the lower range of the evaluated frequencies. It reaches minimum around the DVC cut-off frequency. This implies that the closer the DVC bandwidth is to the bandwidth of the current controller, the more negative is the impact on the passivity of the system. After 300 Hz, the trend is generally towards zero. Hence, increasing the voltage bandwidth could lead to a risk of instability at lower frequencies.

In the case of the MMC, α_v has an impact on all the IAM entries. A higher speed of the ACV results in a wider range of frequencies for which the diagonal entries of the matrix present positive real part. The $Re[Y_{qd}]$ and $Re[-Y_{dq}]$ are also increased

in the same range of frequencies. However, it can be said that at frequencies higher than 250 Hz, the impact of an increase in the controller bandwidth is negligible. For low frequencies the passive behaviour is increased with a higher bandwidth. At higher frequencies the difference is negligible.

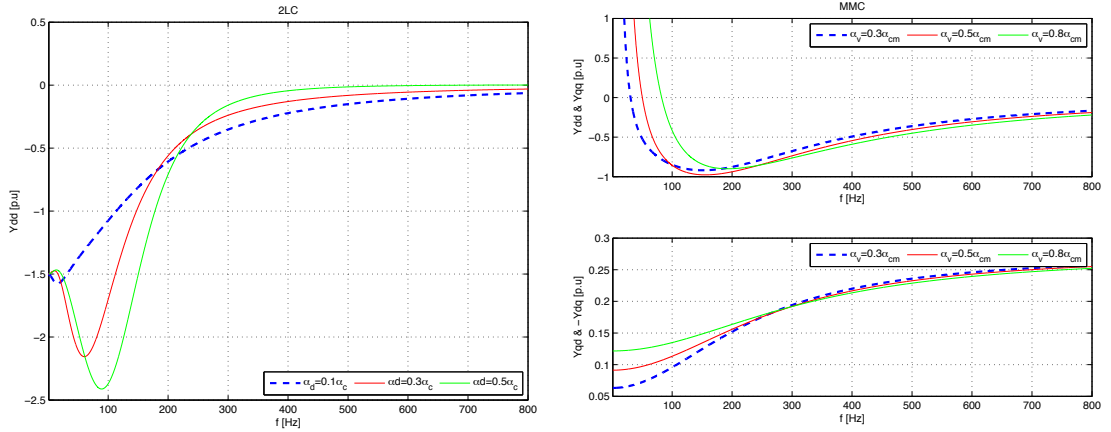


Figure 6.4: Left - Impact of DVC bandwidth on $Re[Y_{dd}(s)]$ of the 2LC. Right - Impact of AVC bandwidth on $Re[Y(s)]$ of the MMC. The blue dashed line demonstrates nominal values.

6.1.4 Impact of passive filtering elements

The filtering elements are key components in the controllers of both converters. Changing the physical elements of the converters might not be feasible in practice, but it is still helpful to evaluate their impact on the conductive behaviour of the system. Therefore, for this assessment the line reactance L_f of the 2LC and the IP capacitor C_f in the MMC model are changed.

The left plot of Fig. 6.5 shows that the passivity of the 2LC increases with the size of L_f . This behaviour is also evident by the ACC transfer function: $Y_i(s) = -\frac{s}{L_f(s+\alpha_c)(s+\alpha_f)}$. It can be said that increasing the size of L_f goes in favour of the passivity of the system.

In the case of the MMC, a change of the C_f has different impacts on the matrix entries. In the right plot of Fig. 6.5 it is shown that the $Re[Y_{dd}(s)]$ and $Re[Y_{qq}(s)]$ get more negative as the size of C_f is increased. On the contrary, the non-diagonal elements become more passive when C_f is reduced.

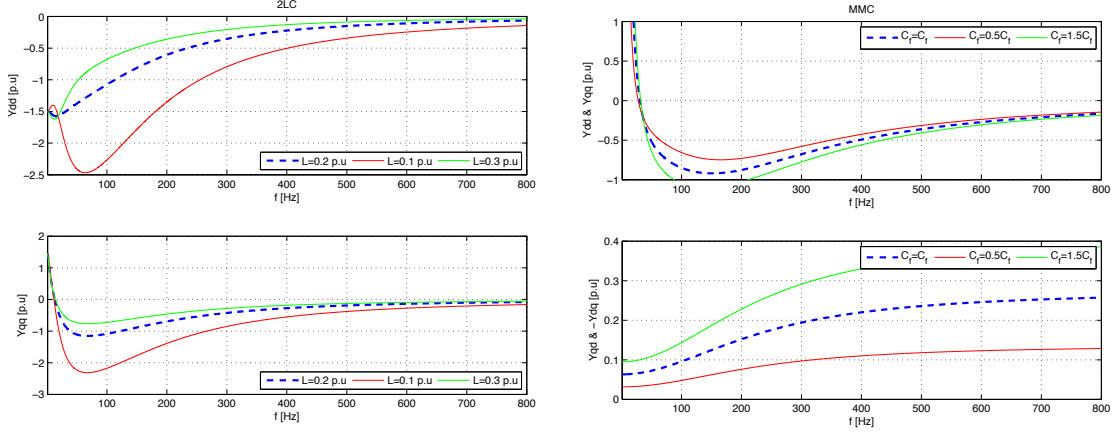


Figure 6.5: Left - Impact of L on the $Re[Y(s)]$ of the 2LC. Right - Impact of C_f on the $Re[Y(s)]$ of the MMC. The blue dashed line demonstrates nominal values.

The analysis should solely give an idea about how the the controller design of the converter has an impact on the passivity of the individual converter.

Note, that if a parameter turns the system more or less passive gives no conclusive statement about the whole system which is studied in this thesis. If a changed bandwidth decreases the passivity gives solely a *hint* on *possible* instability.

6.2 Stability of the Network

The OWF modelled in this project is comprised by the two converters - which passivity was studied in the previous section- and an ac grid, connecting the two elements. The studied closed-loop system in Fig. 6.6 and its two transfer functions $Z_{ac-syst}(s)$ and $Y_{MMC}(s)$ has been obtained earlier.

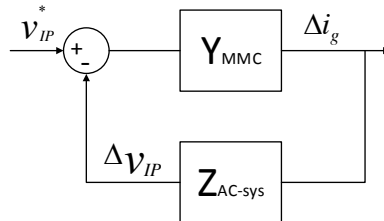


Figure 6.6: Closed loop representation of the evaluated system

The ac-grid impedance $Z_{ac-syst}(s)$ comprises the total ac network system and the 2LC and the MMC admittance $Y_{MMC}(s)$ includes simply the MMC admittance. As previously mentioned, the stability of the OWF can be evaluated according two different approaches: passivity and net-damping criterion.

6.2.1 Passivity analysis

The passivity approach applied in the previous section can be extended to a SISO closed loop system, but only if *both* subsystems are

1. stable and
2. $Re [Z_{ac-syst}(s)] \geq 0$ and $Re [Y_{MMC}(s)] \geq 0$ for $\omega \geq 0$.

It was already shown previously that the transfer function $Y_{MMC}(s)$ is stable. It was also proven, that the 2LC in itself is stable as well, but not yet in connection with the ac cable system. In Fig. 6.7 the poles of the ac system $Z_{ac-syst}(s)$ are plotted. There are multiple poles at zero and also poles which are rather poorly damped. From this plot a marginally stable system can be assumed.

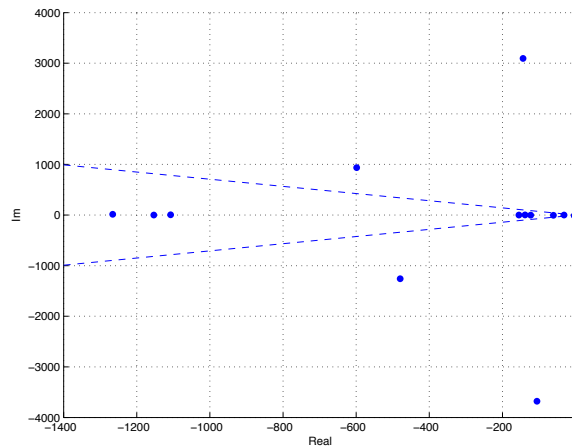


Figure 6.7: Poles of $Z_{ac-sys}(s)$

In order to check the second requirement for passivity, their individual real parts are evaluated, which are displayed in Fig. 6.8.

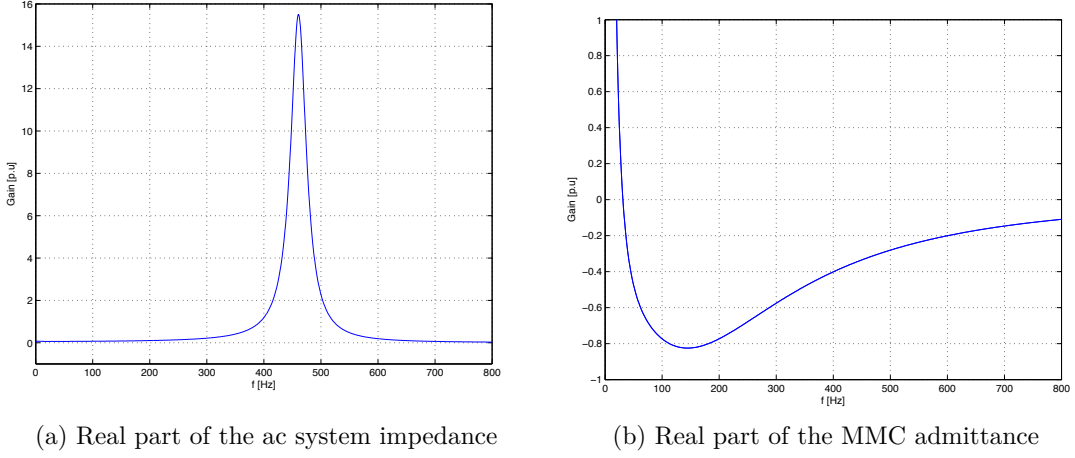


Figure 6.8: Real parts of the studied subsystems

The real part of $Z_{ac-syst}(s)$ is clearly positive over the whole frequency range. However, the $Re[Y_{MMC}(s)]$ shows a rather non-passive behaviour. The two above mentioned requirements are not fulfilled so the passivity study cannot give a final conclusion about the stability of the system. The net-damping stability criterion mentioned in previous Chapters is used for further system analyses.

6.2.2 Net-damping stability criterion

The net-damping criterion is a useful tool since its applicability reaches further than the passivity analysis. For applying this tool no preconditions as stability or passivity are required for the individual subsystems. This method considers that even when both sub models are non-passive or unstable, the closed loop system is not necessarily unstable.

Considering the total SISO closed loop system, (presented in Fig. 6.6) the individual subsystem can be expressed as

$$\frac{1}{Y_{MMC}(j\omega)} = Z_{MMC}(j\omega) = R_{MMC}(\omega) + jX_{MMC}(\omega) \quad (6.1)$$

and

$$Z_{ac-sys}(j\omega) = R_{ac-sys}(\omega) + jX_{ac-sys}(\omega) \quad (6.2)$$

$R_{MMC}(\omega)$ and $R_{ac-sys}(\omega)$ are the real parts of the MMC impedance and the AC-system impedance, and can be seen as the electrical damping of the subsystems. $X_{MMC}(\omega)$ and $X_{ac-sys}(\omega)$ represent their imaginary parts.

The frequencies which should be carefully examined are found at the open-loop resonances. These can be obtained by looking at the gains of the subsystems. In Fig. 6.9 the gains of $Y_{MMC}(j\omega)$ and $Z_{MMC}(j\omega)$ are plotted in p.u., where resonance peaks can be observed in both systems. For the AC system impedance resonance peaks are observed at frequencies $f_{res,1} = 0 \text{ Hz}$, and $f_{res,2} = 462 \text{ Hz}$. The MMC system shows resonance at the frequencies of $f_{res,3} = 0 \text{ Hz}$ and a resonance can be identified around $f_{res,4} \approx 100 \text{ Hz}$.

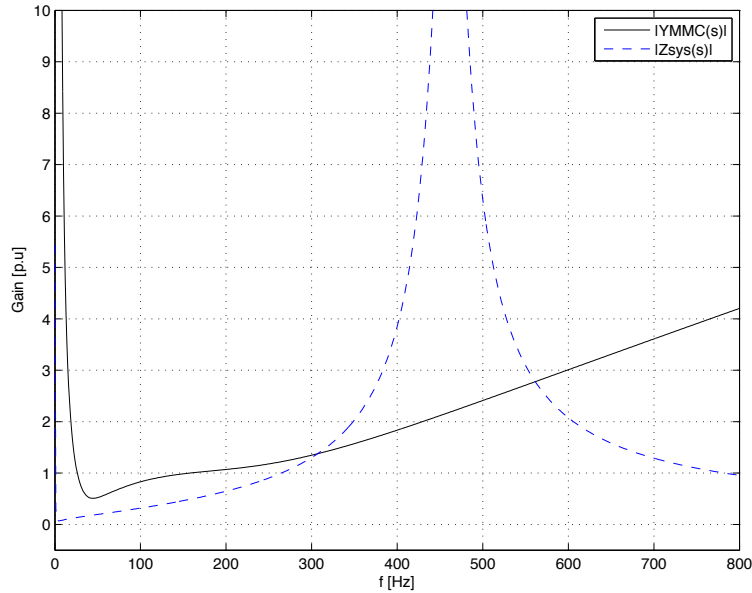


Figure 6.9: Gains of Y_{MMC} and Z_{ac-sys}

When concluding about the resonance origin, it should be kept in mind that this analysis is performed in dq -frame. Hence, the resonance frequencies transformed in the 3-phase system result in $f'_{res,1,3} = 50 \text{ Hz}$, $f'_{res,2} = 512 \text{ Hz}$ and $f'_{res,4} = 150 \text{ Hz}$. The origin of the resonances at $f_{res,1,4} = 0 \text{ Hz}$, which corresponds to the actual operation frequency at 50 Hz, is due to the current controller, in the converters. A similar behaviour is seen in [12] and [17] where the implemented current controller have similar structure as used for the converters modelled in this project.

The resonance around $f_{res,4} = 100 \text{ Hz}$ is related to a resonance of the MMC subsystem.

The high resonance frequency is mainly related to the transmission system resonance, given by the aggregated value of the L and C components, which is calculated as

$$f_{res} = \frac{1}{2\pi} \sqrt{\frac{1}{LC}} \approx 533 \text{ Hz}, \quad (6.3)$$

where the inductance L is the sum of transformer, collection grid and export cable. The capacitance C is simply the sum of the capacitances in the collection system and export cable. The resulting resonance frequency in 6.3 relates not exactly to the resonance peak, which is visible in the graphs. Presumably, the resonance is shifted due to the presence of the 2LC. Even though it results not in the exact value, the difference is within an acceptable range. Further analysis are performed referring to the dq -resonance frequencies as it is shown in the figures.

Now considering the Nyquist criterion, for stability in the system it has to be guaranteed that the Nyquist plot does not encircle $-1 + j0$. Mathematically the statement is true if

$$\text{Re}[Y_{MMC}(j\omega_{res})] \cdot \text{Re}[Z(j\omega_{res})] > -1 \quad (6.4)$$

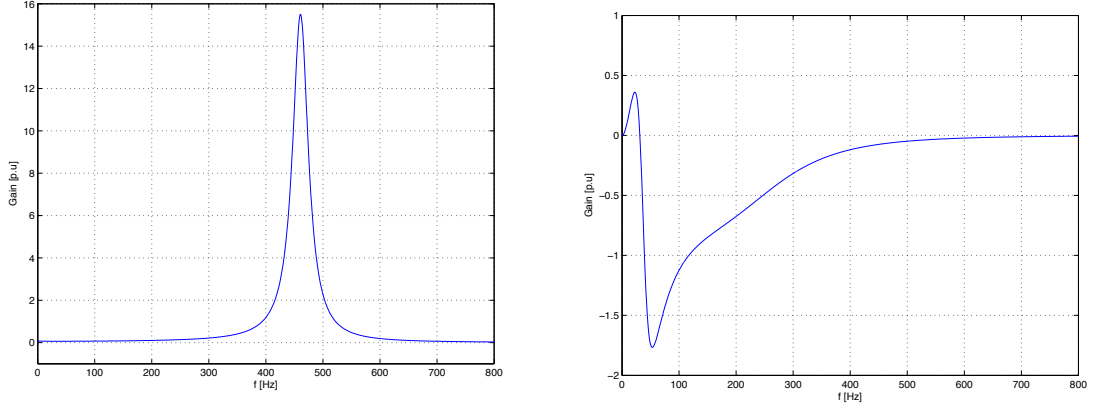
This expression is equivalent to

$$R_G(\omega_{res}) + R_L(\omega_{res}) > 0 \quad (6.5)$$

as it was presented previously in 2.4.2.

In Fig. 6.10 the real part of the two subsystems, R_{MMC} and R_{ac-sys} are plotted to evaluate their properties at the resonance frequency.

Starting with the resonance at $f_{res,1,4} = 0 \text{ Hz}$, both systems $R_{MMC}(0)$ and $R_{ac-sys}(0)$ have a value of zero. This resonance seems to appear in every system including a similar current controller. Only looking into this resonance, the system is said to be marginally stable. However, an investigation at the rest of the resonant frequencies is required to conclude about the stability of the total closed-loop system.


 Figure 6.10: Left - $R_{ac-sys}(s)$; Right - $R_{MMC}(s)$

The resonance observed at $f_{res,4} = 100 \text{ Hz}$ is studied more detailed. For the AC-system the resistive part becomes $R_{ac-sys}(f_{res,4} = 100 \text{ Hz.}) = 0.07 \text{ p.u.}$ whereas the for the MMC it results in $R_{MMC}(f_{res,4} = 100 \text{ Hz.}) = -1.1 \text{ p.u.}$ According to the theory in 2.4.2, the relation in Eq. 6.5 accounts only if $R_{MMC}(\omega_{res}) > 0$. If $R_{MMC}(\omega_{res}) < 0$, which is now the case, the stability criterion is given by the negative net-damping condition:

$$R(\omega_{res}) = R_{MMC}(\omega_{res}) + R_{ac-sys}(\omega_{res}) < 0 \quad (6.6)$$

as derived previously in Chapter 2.

Fig. 6.11 displays the net-damping of both subsystems, and points out the resonance frequencies. From this figure can be concluded that $R(f_{res,4}) < 0$. Consequently it can be claimed that the system is sufficiently damped at this frequency.

Further on, the resonance at $f_{res,3} = 464 \text{ Hz}$ is studied. The resistive parts of the subsystems result in $R_{ac-sys}(f_{res,3} = 464 \text{ Hz.}) = 15.51 \text{ p.u.}$ and $R_{MMC}(f_{res,3} = 495 \text{ Hz.}) = -0.066 \text{ p.u.}$ This means that again negative-net-damping criterion should be applied. The stability criterion for this resonance is given again by Eq. 6.6, since the MMC shows a negative R_{MMC} .

From this the net-damping in Fig.6.11 it is evident that $R(f_{res,3} = 464 \text{ Hz.}) > 0$. Therefore, according to the stability criterion it can be concluded that the closed-loop system of studied network is indeed unstable.

Analysing the conditions leading to instability it is seen that the critical element is

the MMC. Due to the negative damping of this subsystem at the resonant frequency, negative net-damping criterion has to be applied. However, at that critical point, the negative damping of the MMC is not enough to counter the positive damping of the ac-system, and hence the the negative criterion is not fulfilled. It becomes obvious that a CI appears in the studied network. The controllers and design parameter shaping the admittance of the MMC have a negative impact on the network impedance, leading to an instability in the system.

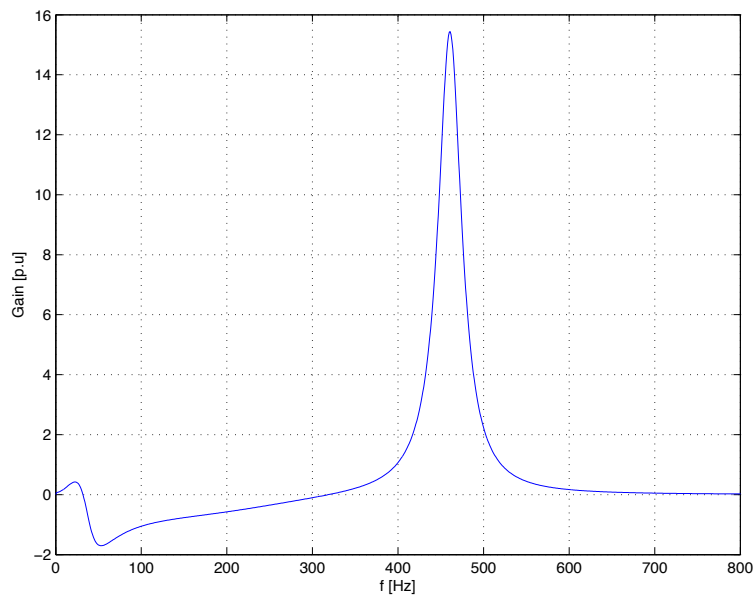
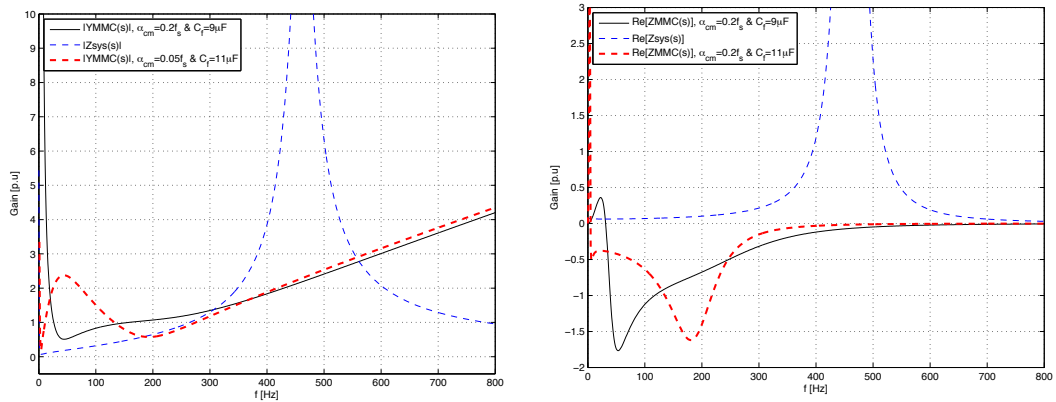
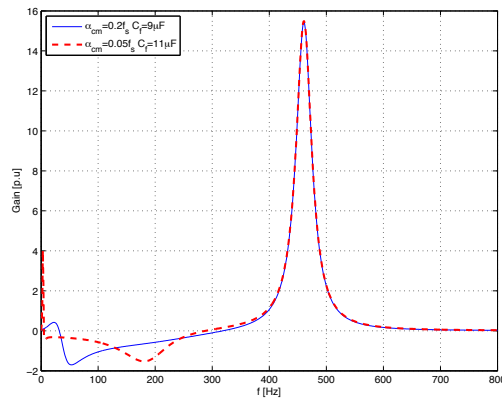


Figure 6.11: Net damping ($Z_{ac-sys}(s) + Z_{MMC}(s)$)

Going back to the results in section 6.1 and focusing on the range of frequencies where the instability is found, it is seen that the admittance of the MMC is negatively affected by high values of the current controller bandwidth and lower capacitance values of the filter C_f . On the other hand, the impact of the AVC around that frequency range is negligible. Hence, in an attempt to change the properties of the MMC admittance in favour of the stability of the system, α_{cm} is decreased and the filter capacitance is increased. Fig. 6.12b shows how the damping of the MMC gets values close to zero but is still slightly negative. According to Eq. 6.6, the system will still be unstable.



(a) Gains of the MMC admittance and ac-system (b) Damping terms $R(s)$ of the two converters impedance



(c) Net damping

Figure 6.12: Impact of parameter variation over the stability of the system according to net-damping criterion

6.2.3 Verification with time-domain simulation

This short section is presenting the result of the time-domain model when applying a perturbation to the system.

The analysis of the previous part states that the closed-loop system is unstable. For this verification a voltage perturbation of 5% of the nominal reference value is inserted in the AVC of the MMC.

In Fig. 6.13 the system response is illustrated for the AVC. A voltage step in v_d is applied at 5s. This results in a poorly damped oscillation that becomes more noticeable around 14s. However, it is also observed that from the time domain simulation, it can not be claimed that the system is unstable.

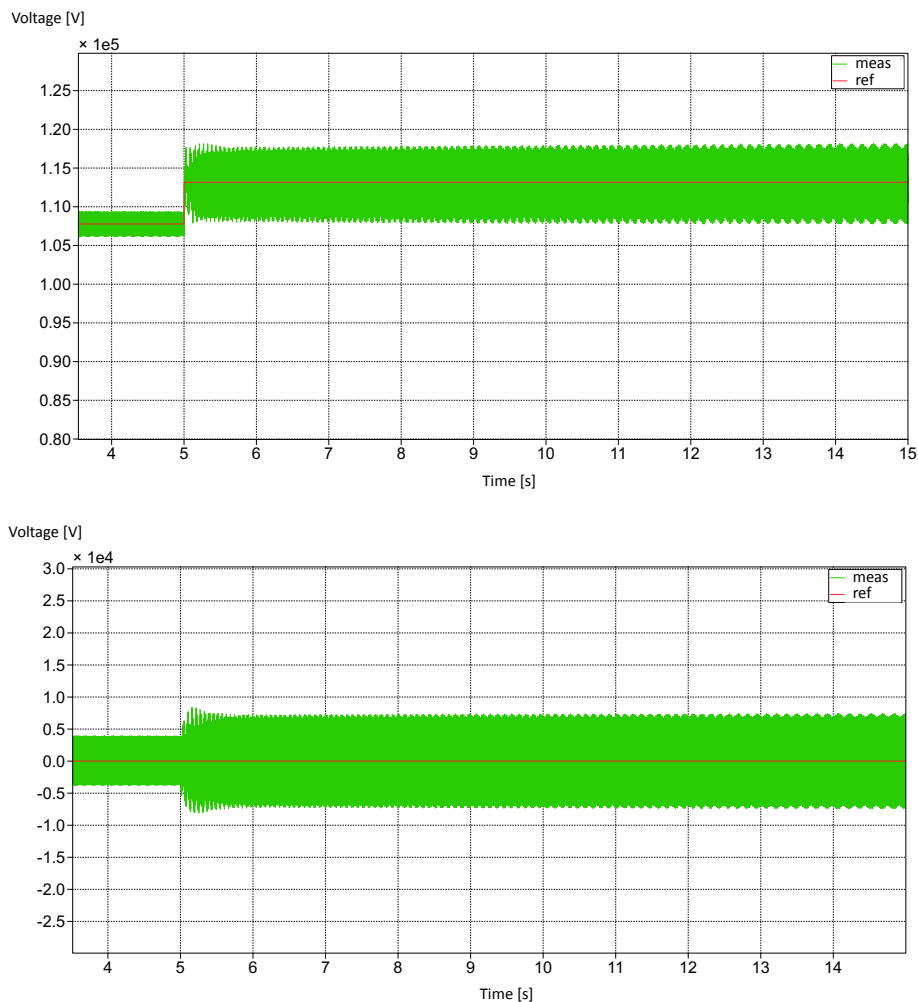


Figure 6.13: Simulation results when inserting a reference voltage step on the MMC side

This last verification shows that the analytical model and the simulation model are not totally consistent. Even though an instability is concluded by means the net damping criterion, a merely poorly damped system is presented in the time-domain simulations.

This discrepancy in results can be due to different reasons. At the resonance frequency of 464 Hz a large difference between the p.u. values can be observed. The ac system is contributing the net-damping value in a large scale, whereas the MMC adds only with a really small negative value. Due to the negative appearance of R_{MMC} the stability criterion was changed from $R(s) > 0$ to $R(s) < 0$. Consequently, a slight shift of R_{MMC} into the positive region would result in the conclusion of a stable system as shown in time domain simulations.

Even though nothing can be concluded about it, there is the chance that by having include delay times in the analytical model the R_{MMC} would be actually shifted up at the resonance frequency and hence matching with the time domain simulation results.

6.3 Method for System Stability Evaluation

The method presented in this section aims for summarising a procedure for conclusive results about the origin of instabilities in a network by analysing the system in frequency-domain. It is based on the study case of this thesis, but it can be extended to any power network in which VSCs are connected. Moreover, the IAM blocks of the 2LC and the MMC derived in this project can be directly used in stability analysis of networks comprising these converters. Only modifications regarding design parameters of the converters might be necessary. Hence, if a similar network is to be evaluated, applying this method and by having two main blocks modelled, the assessment of electrical interactions possibly leading to instabilities can be performed in this way.

The five different processes conforming this analytical method are illustrated in Fig. 6.14 by a colour code. The first process is the characterisation of the system under evaluation, which starts by identifying the elements in the power network that can potentially lead to negative interactions between each other, e.g. VSCs, series compensated lines. The connection of these elements in a closed-loop system should be laid paying special attention to the signs convention. The proper assumptions and simplifications should be taken into account in this step of the characterisation.

Then, the design process should include the system characteristics and represent the elements of the network in frequency-domain.

Once the system is designed for the operation of the elements in the network, the transfer functions of the subsystems and/or their IAM can be obtained. These two representations allow different studies.

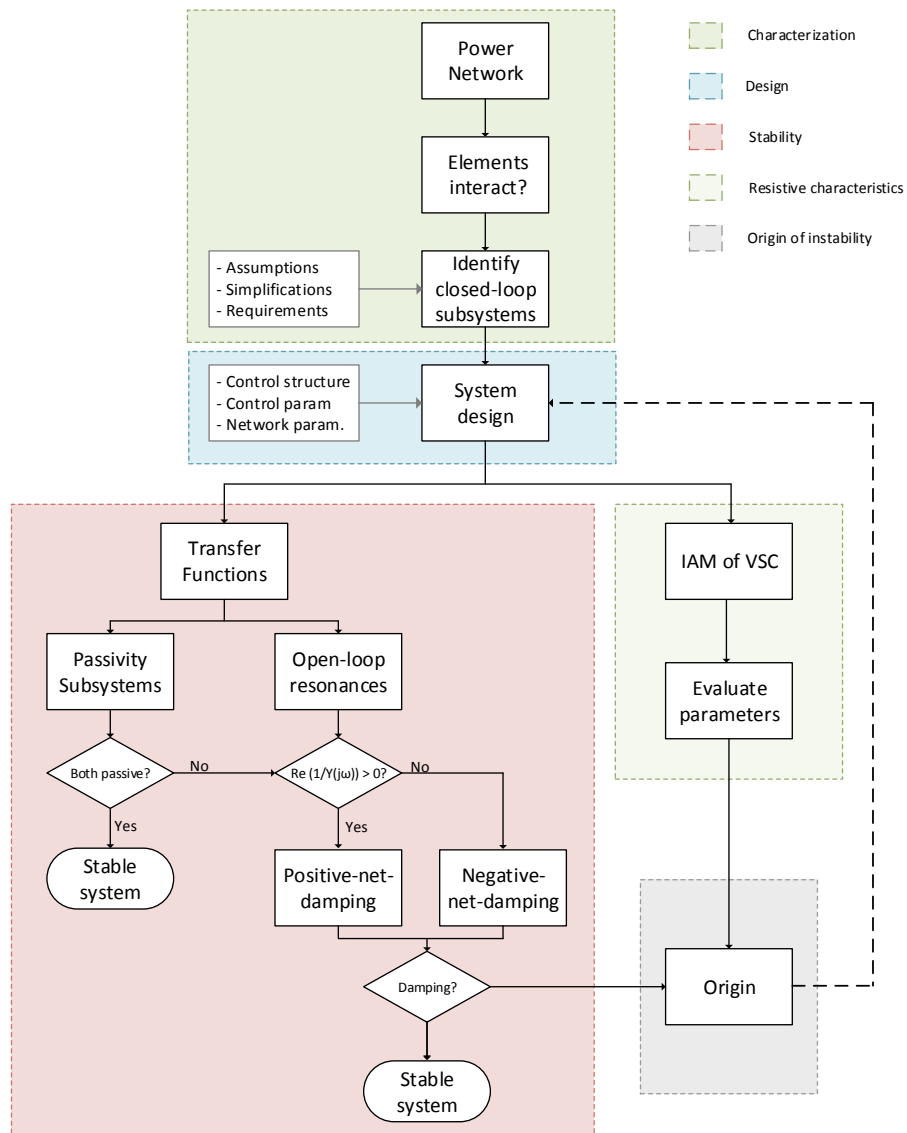


Figure 6.14: Flow chart of analytical method for evaluation of origin of instabilities

The transfer functions of the subsystems in the closed-loop are required in the

process of assessing the stability of the overall system. The flow chart in Fig. 6.14, illustrates that the stability of the whole system can be quickly determined if both subsystems are found to be passive. However, if this is not the case, the network stability should be assessed through the other sub-process. By looking into the open-loop resonances and checking the real part value of the input admittance transfer function $Y(j\omega)$ (not the feedback transfer function) it can be seen whether the positive or the negative net-damping criterion should be applied in the stability evaluation of the network. If through these criteria the system is concluded to be unstable, the information taken from the parallel process is useful to understand the origin of the instability.

Through the process of evaluating the real part of the IAMs of the elements in the network, the impact of the different design parameters over the subsystems impedance can be analysed. Relevant knowledge about the relation between the design parameters and the origin of possible instabilities can be obtained in these analyses.

Finally, to locate the origin of instabilities the information from the real parts of the subsystems used in the net-damping stability criterion, together with the information derived from the IAM, the subsystems behaviour leading to instability can be detected and possible corrected through a re-design of the initial parameters.

6.4 Summary

This Chapter starts with the passivity analysis of the 2LC and the MMC mathematical models. Some design parameters are changed to understand their impact on the IAM passive characteristics. However, no conclusions about the total stability of the system can be drawn from this analysis since the 2LC is analysed individually and not in the aggregated $Z_{ac-sys}(s)$.

The evaluation of the closed-loop system stability is first attempted to analyse by the passivity of the subsystems $Z_{ac-sys}(s)$ and $Y_{MMC}(s)$ according to the criterion. It is found that due to non-passivity of one of the sub-models, nothing can be concluded about the total system.

Since no pre-conditions of passivity or stability of the subsystems is required with the net-damping criterion the closed-loop system of the OWF network is analysed and it is concluded that the system is indeed unstable. By applying the

Nyquist criterion to the open-loop transfer function $G_{ol}(s) = Z_{ac-sys}(s) \cdot Y_{MMC}(s)$ and analysing the damping coefficients of each subsystem at critical frequencies, the subsystem with negative impact over the net-damping of the system can be identified. Through the IAM passivity analysis facilitates the possible redesign for ensuring system stability. Independently of the actual stability of the system, this analysis is also helpful to detect hints for instability in case that the design parameters are modified.

Finally, a method for obtaining conclusive answers about the stability of the closed-loop function of a network is derived and presented in a flow-chart.

7 Conclusion and Future Work

7.1 Conclusion

This thesis presents a methodology which offers a systematic approach for the investigation of possible instabilities in an OWF network with different VSCs technologies. In Chapter 6 a discrepancy between the analytical results and the time domain simulation is found. This puts into question the validity of the simplifications made in the modelling process and the exactitude of the procedure to aggregate the different parts of the network.

The methodology is based on the study case of this project where the elements influencing the network stability are the full-scale-power converter of a WT, an MMC-based HVDC station and the offshore network connecting these units.

The different processes involved in the presented methodology are addressed through the Chapters of this the report, starting from the basic theory behind modelling the elements in the network for stability studies purposes. This theory is presented in Chapter 2, as well as the several assumptions and simplifications found in other stability studies in networks similar to the one investigated in this project. This brief research shows that the modelling of the power networks through IAMs offers great advantages when assessing origin of instabilities in the system. Also, a review of the passivity and net-damping criteria shows that both tools can be useful for concluding about the stability of the studied network.

Chapter 3 describes the general operation of the benchmark OWF and highlights the most relevant assumptions for the modelling of the system by presenting the single-line diagram of the simplified system. Moreover, for the purpose of the study, the network is divided into two subsystems, which can be assessed in closed-loop. At this point, it is noticed that an obvious sign convention should be kept during the different stages of the study. It is also crucial to carefully decide which elements will comprise the subsystems. If only the interaction of the converter with the network is studied, the subsystems can be easily defined. However, this task gets

more complex when the passive elements in the network should be aggregated with a controlled admittance. This in fact is a possible reason for the non consistent results obtained in this thesis.

Later, Chapter 4 moves on with the design of the elements in the network. Special attention is given in deriving the mathematical expressions that describe the operation of the controllers in each of the converters, since the possible interaction of these subsystems is sourced in the layout of this equations. The simplification process for modelling the ac transmission system of the wind farm is also explained in this Chapter.

The construction of the subsystems previously identified is presented in Chapter 5. Here, the IAM of both converters is obtained as well as their correspondent transfer functions. It is mentioned that these two representations of the same system can be used for different purposes and both are contemplated in the methodology derived in the project. However, The 2LC IAM is further aggregated with the ac network to shape one of the subsystems in the closed-loop scheme. The other subsystem is just comprised by the admittance of the MMC. A verification of the converter models is carried out by means of time domain simulations. The trend of the admittances of both converters is verified for the studied frequency range and the correct operation of the system is evaluated in time domain simulations. However, the impedance of the aggregated ac-system (2LC and network) is not verified, leaving uncertainties for the root of the discrepancy in the stability properties of the system between analytical results and time domain simulations.

Finally, in Chapter 6 the possibility of CI is assessed. The passivity approach is applied to demonstrate the impact of individual design parameters on the converters IAMs. With this study it is possible to identify the contribution of the parameters to the passivity of the converters for a given frequency range. However, no conclusion about the stability of the whole system can be obtained from this first analysis since the ac network is not included. An attempt to apply the passivity approach to study the closed-loop system. However, due to the non-passive behaviour of the MMC admittance, it is found that the passivity approach cannot give a conclusive answer about the stability of the system. By means of the net-damping criterion the closed-loop system of the OWF network is analysed and conclusive independently of the conditions of the individual subsystems. In this case, the closed-loop system is found to be unstable and CI in the network is analytically confirmed. However, time-domain simulations do not confirm this fact.

From what is previously stated it can be concluded that the objectives of the project have been partially fulfilled:

- The control structures of each of the converters are derived.
- The IAMs of both converters are obtained based on the implemented control structures .
- The influence of the design parameter on the IAM of the converters is analysed and useful information for detecting the origin of instability is obtained.
- Analytically, it is determined that CI in the network exists and leads to stability problems in the OWF network. However, the discrepancy with the results obtained by means of time-domain simulations prevents from drawing a final conclusion about the stability of the system.

7.2 Future Work

In the conclusions of this thesis it is mentioned that the aggregated model of the network and the 2LC might have been not accurate enough.

- For future studies one can research an approach of combining passive elements of a cable network with a transfer function including an active controller.
- The individual subsystems should be verified in a more proper way so that during later analyses accurate conclusions can be drawn without querying the derived analytical model

No precise conclusion about the system stability could be drawn in this thesis. One could research if the reason for this mismatch is based on the choice of elements included in the subsystems derived for the closed-loop system analysis.

- Conclusions could be proven by deriving a SISO closed loop with rearranged subsystems. One system could be based only on the 2LC, while the other subsystem includes the MMC combined with the ac network.
- Regarding the net damping criterion it could be proven mathematically that the final conclusion is independent of the arrangement of components to the subsystems.

By the time of finalising this thesis, grid codes within the OWF network have are not yet in force.

- In a future study one could research on new requirements and may adapt the design of the controller or implement additional equipment.

The system design was held rather simple in this thesis. Future projects could be based on increased network complexity. One could include

- A higher number of WTs including their back-to-back converter instead of aggregating to one single component.
- Longer cables, which might imply the reactive power control by the 2LC for voltage support along the ac transmission system.

Bibliography

- [1] ABB. *XLPE Submarine Cable Systems*.
- [2] Jakob Glasdam, Jesper Hjerrild, Lukasz Hubert Kocewiak, and Claus Leth Bak. Review on multi-level voltage source converter based hvdc technologies for grid connection of large offshore wind farms. In *Power System Technology (POWERCON), 2012 IEEE International Conference on*, pages 1–6. IEEE, 2012.
- [3] UN Gnanarathna, Sanjay Kumar Chaudhary, AM Gole, and Remus Teodorescu. Modular multi-level converter based hvdc system for grid connection of offshore wind power plant. In *AC and DC Power Transmission, 2010. ACDC. 9th IET International Conference on*, 2010.
- [4] Kong Xiangyu and Jia Hongjie. Techno-economic analysis of svc-hvdc transmission system for offshore wind. In *Power and Energy Engineering Conference (APPEEC), 2011 Asia-Pacific*, pages 1–5. IEEE, 2011.
- [5] Hanchao Liu and Jian Sun. Voltage stability and control of offshore wind farms with ac collection and hvdc transmission. 2014.
- [6] Anton Lesnicar and Rainer Marquardt. An innovative modular multilevel converter topology suitable for a wide power range. In *Power Tech Conference Proceedings, 2003 IEEE Bologna*, volume 3, pages 6–pp. IEEE, 2003.
- [7] N-T Trinh, Marcus Zeller, Klaus Wuerflinger, and István Erlich. Generic model of mmc-vsc-hvdc for interaction study with ac power system. 2015.
- [8] R Nath and C Grande-Moran. Study of sub-synchronous control interaction due to the interconnection of wind farms to a series compensated transmission system. In *Transmission and Distribution Conference and Exposition (T&D), 2012 IEEE PES*, pages 1–6. IEEE, 2012.
- [9] Khaled Mohammad Alawasa, YA-RI Mohamed, and Wilsun Xu. Active mitigation of subsynchronous interactions between pwm voltage-source converters and power networks. *Power Electronics, IEEE Transactions on*, 29(1):121–134, 2014.

- [10] Lennart Harnefors, Massimo Bongiorno, and Stefan Lundberg. Stability analysis of converter-grid interaction using the converter input admittance. In *Power Electronics and Applications, 2007 European Conference on*, pages 1–10. IEEE, 2007.
- [11] Georgios Stamatiou. *Converter interactions in VSC-based HVDC systems*. PhD thesis, Chalmers University of Technology, 2015.
- [12] HT Ma, PB Brogan, KH Jensen, and RJ Nelson. Sub-synchronous control interaction studies between full-converter wind turbines and series-compensated ac transmission lines. In *Power and Energy Society General Meeting, 2012 IEEE*, pages 1–5. IEEE, 2012.
- [13] S.P. Teeuwsen, R. Zurowski, Li-Jun Cai, S. Jensen, A. Osmanbasic, and F. Gafaro. Transient interaction study for vsc-hvdc connected offshore wind park considering original controls. In *PES General Meeting / Conference Exposition, 2014 IEEE*, pages 1–5, July 2014.
- [14] Thanh Hai Nguyen and Dong-Choon Lee. Control of offshore wind farms based in hvdc. In *Energy Conversion Congress and Exposition (ECCE), 2012 IEEE*, 2012.
- [15] Christian Ismunandar. *M.Sc. Thesis. Control of Multi-Terminal VSC-HVDC for Offshore Wind Power Integration*. Department of Electrical Sustainable Energy, August, 2010.
- [16] J.G. Slootweg and W.L. Kling. The impact of large scale wind power generation on power system oscillations. *Electric Power Systems Research*, 67, 2003.
- [17] Hanchao Liu and Jian Sun. Impedance-based stability analysis of vsc-based hvdc systems. In *Control and Modeling for Power Electronics (COMPEL), 2013 IEEE 14th Workshop on*, pages 1–8, June 2013.
- [18] R. da Silva, R. Teodorescu, and P. Rodriguez. Power delivery in multiterminal vsc-hvdc transmission system for offshore wind power applications. In *Innovative Smart Grid Technologies Conference Europe (ISGT Europe), 2010 IEEE PES*, pages 1–8, Oct 2010.
- [19] Andrzej Adamczyk. *Damping of Low Frequency Power System Oscillations with Wind Power Plants*. PhD thesis, 2012.
- [20] Gustavo Pinares. *On the Analysis of DC Network Dynamics of VSC-based HVDC Systems*. PhD thesis, 2014.
- [21] Mi Sa Nguyen Thi and Li Wang. Stability analysis of power transmission of offshore wind farms fed to onshore power grids using a multi-terminal

- vsc-hvdc system. In *Circuits and Systems (APCCAS), 2012 IEEE Asia Pacific Conference on*, pages 575–578, Dec 2012.
- [22] Lennart Harnefors, M. Bongiorno, and S. Lundberg. Input-admittance calculation and shaping for controlled voltage-source converters. *Industrial Electronics, IEEE Transactions on*, 54(6):3323–3334, Dec 2007.
- [23] Lennart Harnefors. Modeling of three-phase dynamic systems using complex transfer functions and transfer matrices. *Industrial Electronics, IEEE Transactions on*, 54(4):2239–2248, Aug 2007.
- [24] Lennart Harnefors. Proof and application of the positive-net-damping stability criterion. *Power Systems, IEEE Transactions on*, 26(1):481–482, Feb 2011.
- [25] H.K. Müller, S. Shariat Torbaghan, M. Gibescu, M.M. Roggenkamp, and M.A.M.M. van der Meijden. The need for a common standard for voltage levels of hvdc-vsc technology. *Energy Policy*, 63(0):244 – 251, 2013.
- [26] Entso-e draft network code on high voltage direct current connections and dc-connected power park modules.
- [27] E Muljadi, CP Butterfield, A Ellis, J Mechenbier, J Hochheimer, R Young, N Miller, R Delmerico, R Zavadil, and JC Smith. Equivalencing the collector system of a large wind power plant. In *Power Engineering Society General Meeting, 2006. IEEE*, pages 9–pp. IEEE, 2006.
- [28] National Electricity Transmission System Security and Quality of Supply Standard, 2012.
- [29] Narain G Hingorani, Laszlo Gyugyi, and Mohamed El-Hawary. *Understanding FACTS: concepts and technology of flexible AC transmission systems*, volume 1. IEEE press New York, 2000.
- [30] Jian Sun. Small-signal methods for ac distributed power system- a review. *Power Electronics, IEEE Transactions on*, 21-11:2545–2554, 2009, Nov.
- [31] Frede Blaabjerg, Marco Liserre, and Ke Ma. Power electronics converters for wind turbine systems. *IEEE Transactions on Industry Applications*, 48(2), March/April 2012.
- [32] Remus Teodorescu, Marco Liserre, and Pedro Rodriguez. *Grid converters for photovoltaic and wind power systems*, volume 29. John Wiley & Sons, 2011.
- [33] Lennart Harnefors and M. Bongiorno. Current controller design for passivity of the input admittance. In *Power Electronics and Applications, 2009. EPE '09. 13th European Conference on*, pages 1–8, Sept 2009.

- [34] Michael Lindgren. *Modeling and control of voltage source converters connected to the grid*. Chalmers University of Technology, 1998.
- [35] Nicolás Espinoza, Massimo Bongiorno, and Ola Carlson. Grid code testing of full power converter based wind turbines using back-to-back voltage source converter system. In *EWEA Annual Event 2013 conference proceedings*, 2013.
- [36] M. Saeedifard and R. Iravani. Dynamic performance of a modular multilevel back-to-back hvdc system. In *Power and Energy Society General Meeting, 2011 IEEE*, pages 1–1, July 2011.
- [37] G.P Adam, S.J Finney, K.H Ahmed, and B.W Williams. Modular multilevel converter modeling for power system studies. *Power Engineering, Energy and Electrical Drives (POWERENG)*, 2013.
- [38] Jaime Peralta, Hani Saad, Sébastien Denetière, Jean Mahseredjian, and Samuel Nguefeu. Detailed and averaged models for a 401-level mmc-hvdc system. *Transactions on Power delivery*, 27(3), 2012.
- [39] Prabha Kundur, Neal J Balu, and Mark G Lauby. *Power system stability and control*, volume 7. McGraw-hill New York, 1994.
- [40] Sanna Uski. Wind power plant model collection network representation in an aggregated wind power plant model. Technical report, VTT Technical Research Centre of Finland.
- [41] M Ragheb. Orography and wind turbine siting. *Viiattu*, 15, 2012.
- [42] Gamesa 5.0 mw innovating for reliability. Technical report, February 2015.
- [43] KR Padiyar. *Analysis of subsynchronous resonance in power systems*, volume 471. Springer Science & Business Media, 1998.
- [44] F.Wang, L. Bertling, T. Ahn Le, A. Mannikoff, and A. Bergman. An overview introduction of vsc-hvdc: State-of-art and potential applications in electric power systems. *Cigrè International Symposium, Bologna, Italy*, September 2011.

A Appendix

A.1 $dq0$ Reference frame

Commonly, in 3-phase VSC linear PI controller are used based on the vector current control method in the dq -synchronous frame [44]. In the dq -system, three phase quantities are transformed in two dc quantities for reducing complexity and simplifying equations. Applying Clarke transformation, the three phases of a , b , and c can be converted to the $\alpha\beta\gamma$ system, where γ is equal to zero in symmetric systems. Further, Park transformation ($dq0$) results in one vector rotating in the stationary $\alpha\beta\gamma$ frame. This reference frame is commonly used to simplify the analyses in electrical systems and is defined by

$$u_{dq}(t) = u_d(t) + ju_q(t) = u_{\alpha\beta}(t)e^{-j\theta(t)} \quad (\text{A.1})$$

where θ is the angle of the rotating system. The zero component of $dq0$ is comparable with the γ component, however it is disregarded in this project since only symmetric systems are considered. Ideally, the dq reference frame is rotating at the grid frequency ω_g with an angle $\theta = 0$. This phasors are illustrated in Fig. A.1 [20][32]. The power in the dq reference frame is calculated as

$$S = P + jQ = \frac{2}{3} \cdot u_{dq} \cdot i_{dq} \quad (\text{A.2})$$

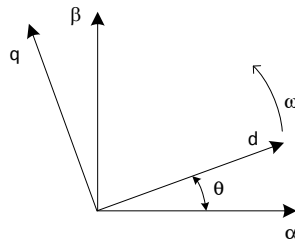


Figure A.1: Phasors $\alpha\beta$ to dq transformation

and can be divided into active and reactive power as

$$P = \frac{2}{3}(u_d i_d + u_q i_q) \quad Q = \frac{2}{3}(-u_d i_q + u_q i_d) \quad (\text{A.3})$$

In steady state the d component v_d is aligned with phase a of the grid voltage V_{abc} and equals the voltage amplitude V_m . Thus v_q is zero in steady state operation. This changes equation A.3 to:

$$P = \frac{2}{3}u_d i_d \quad Q = -\frac{2}{3}u_d i_q \quad (\text{A.4})$$

Eq. A.4 demonstrates the decoupling of P and Q control if the systems are perfectly synchronised. P is controlled with i_d whereas Q depends only on i_q .